In-situ estimation of subsurface hydro-geomechanical properties using the groundwater response to semi-diurnal Earth and atmospheric tides

Gabriel C. Rau[1,2], Timothy C. McMillan[3,4], Martin S. Andersen[3], and Wendy A. Timms[5]

[1]School of Environmental and Life Sciences, The University of Newcastle, Newcastle, Australia
[2]Institute of Applied Geosciences, Karlsruhe Institute of Technology, Karlsruhe, Germany
[3]School of Civil and Environmental Engineering, The University of New South Wales, Sydney, Australia
[4]School of Mineral and Energy Resource Engineering, The University of New South Wales, Sydney, Australia
[5]School of Engineering, Deakin University, Waurn Ponds, Australia

Correspondence: Gabriel C. Rau (gabriel.rau@newcastle.edu.au)

Abstract. Subsurface hydro-geomechanical properties crucially underpin the management of Earth's resources, yet they are predominantly measured on core-samples in the laboratory while little is known about the representativeness of in-situ conditions. The impact of Earth and atmospheric tides on borehole water levels are ubiquitous and can be used to characterise the subsurface. We illustrate that disentangling the groundwater response to Earth (M_2) and atmospheric tidal (S_2) forces in
5   conjunction with established hydraulic and linear poroelastic theories leads to a complete determination of the whole hydro-geomechanical parameter space for unconsolidated systems. Further, the characterisation of consolidated systems is possible when using literature estimates of the grain compressibility. While previous field investigations have assumed a Poisson's ratio from literature values, our new approach allows for its estimation under in-situ field conditions. We apply this method to water level and barometric pressure records from four field sites with contrasting hydrogeology. Estimated hydro-geomechanical
10   properties (e.g. specific storage, hydraulic conductivity, porosity, shear-, Young's- and bulk- moduli, Skempton's and Biot-Willis coefficients and undrained/drained Poisson's ratios) are comparable to values reported in the literature, except for consistently negative drained Poisson's ratios which are surprising. Our results reveal an anisotropic response to strain, which is expected for heterogeneous (layered) lithological profiles. Closer analysis reveals that negative Poisson's ratios can be explained by differing in-situ conditions to those from typical laboratory core tests and the small strains generated by Earth
15   and atmospheric tides. Our new approach can be used to passively, and therefore cost-effectively, estimate subsurface hydro-geomechanical properties representative of in-situ conditions and improves our understanding of the relationship between geological heterogeneity and geomechanical behaviour.

1 Introduction

20 A perpetual challenge for subsurface water, mineral resource or geotechnical projects is a proper characterisation of the physical properties that may have bearings on the rate of resource extraction, operation, safety and environmental impact of the project. The main reason for this challenge is the subsurface's heterogeneous nature and that the sampling density necessary to describe it may be prohibitively expensive (e.g. by drilling and testing of core). This issue is further exacerbated by the difficulty in approximating in-situ environments in laboratory testing in regards to both scale and subsurface pressures (Hoek and

25 Diederichs, 2006; Cundall et al., 2008; Bouzalakos et al., 2016). These difficulties may be overcome by in-situ characterisation of hydro-geomechanical properties of the subsurface (Villeneuve et al., 2018). Here, the in-situ pressure, stress conditions, and the scaling and inclusion of heterogeneities can achieve a more representative estimate than possible from selective laboratory testing.

Detailed time-series analysis of water table fluctuations in boreholes due to Earth and atmospheric tides (EAT) has been

30 shown to be capable of deriving hydro-geomechanical properties (Hsieh et al., 1987; Rojstaczer and Agnew, 1989; Zhang et al., 2019). Further, with assumed values of some key variables, previous authors have also been able to extend the use of EAT to estimate additional subsurface hydro-geomechanical properties (Bredehoeft, 1967; Beavan et al., 1991; Cutillo and Bredehoeft, 2011). However, methods which use EAT, referred to as tidal subsurface analysis (TSA) techniques, remains underutilised.

35 EAT are natural phenomena, causes by celestial bodies (e.g., Sun or Moon), that occur throughout the Earth's crust, which have been measured and analysed in the subsurface since the mid-20th century (McMillan et al., 2019). Traditionally these techniques have focused on either Earth tides (ET) (Bredehoeft, 1967; Hsieh et al., 1987; Cutillo and Bredehoeft, 2011; Zhang et al., 2019; Burbey, 2010), barometric pressure (Clark, 1967; Cutillo and Bredehoeft, 2011) or atmospheric tide (AT) loading (Acworth et al., 2016; McMillan et al., 2019; Rau et al., 2020) of the confined subsurface. Bredehoeft (1967) first proposed that

40 once specific storage is calculated from the groundwater response to Earth tides, an aquifer porosity and compressibility can be determined from the formation pressure response to a uniformly distributed surface load such as caused by barometric pressure changes (Narasimhan et al., 1984; Rojstaczer, 1988; Rojstaczer and Riley, 1990; Ritzi et al., 1991; Burbey et al., 2012). This concept has been reiterated in the literature but, to the best of our knowledge, never solved without the use of either an assumed Poisson's ratio or bulk modulus (Cutillo and Bredehoeft, 2011) due to difficulties in attributing the superimposed EAT effects

45 to their respective drivers (e.g. celestial body gravitational or atmospheric loading forces). Recent work by Rau et al. (2020) compares methods that estimate amplitudes and phases from monitoring datasets and concludes that *harmonic least squares* (HALS) is superior compared to *Fast Fourier Transforms* (FFT).

In this paper, the theory of the groundwater response to Earth and atmospheric tides is combined, thereby providing a new methodology for the estimation of the primary subsurface hydrogeomechanical properties (storage, hydraulic conductivity

50 and poroelastic properties). This new method improves upon the work of Cutillo and Bredehoeft (2011), as it quantitatively disentangles the groundwater response to Earth and atmospheric tides within the frequency domain, removing the influence from non-harmonic signals (e.g. precipitation and episodic recharge events) and allowing the separate and objective estimation

Tidal component (Darwinian name)	Frequency (cpd)	Tidal potential $(m^2 s^{-2})$	Tidal gravity variation $(m s^{-2})$	Tidal dilatation / areal strain $(-)$	Description	Attribution
M_2	1.932274	42.060943	$6.477 \cdot 10^{-5}$	$2.625 \cdot 10^{-7}$	Principal lunar semi-diurnal	Earth
S_2	2.000000	19.309855	$2.973 \cdot 10^{-5}$	$1.205 \cdot 10^{-7}$	Principal solar semi-diurnal	Atmosphere/Earth

Table 1. Table of M_2 and S_2 tidal components, tidal potential, gravity and dilatation using tidal predictions (this does not include local variations). Extracted from Agnew (2010) and McMillan et al. (2019).

of properties from each driver before combining the strain responses. Here, the hydraulic and linear poroelastic works of Hsieh et al. (1987), Rojstaczer and Agnew (1989), Beavan et al. (1991) and Rau et al. (2020) are integrated and combined, leading to a complete determination of the parameter space for unconsolidated systems. Further, the characterisation of consolidated systems is possible when using literature estimates of the grain compressibility (van der Kamp and Gale, 1983; Green and Wang, 1990). Finally, the new methodology is applied to groundwater and atmospheric pressure records in five boreholes from four sites to estimate hydrogeological and geomechanical properties of various consolidated and unconsolidated stratigraphies.

2 Theoretical background

2.1 Extracting tidal components

Atmospheric heating and the gravitational pull of celestial bodies exert a loading of the Earth's crust (Agnew, 2010). The gravity variations and loading exerted by the movement of these celestial bodies (i.e., the Moon and Sun), as shown in Table 1, cause stress and strain responses in the Earth's crust. This causes a subsurface strain signal that is composed of numerous superimposed signals of various frequencies and amplitudes. For undrained conditions (pressurised) of either confined or semi-confined aquifers, this strain manifests as a groundwater pore pressure fluctuation (McMillan et al., 2019). A conceptual illustration of these processes is shown in Figure 1.

Three variables are required to calculate subsurface properties using specific harmonic components (McMillan et al., 2019): (1) a computed dilatation or strain due to Earth tides (denoted by the superscript ET); (2) measured barometric pressure (denoted by the superscript AT in later equations); and (3) measured groundwater heads (denoted by the superscript GW). First, a moving average spanning across a time period of 3 days is applied. The tidally induced frequency components are then extracted by using *harmonic least-squares* (HALS) to estimate the harmonic components caused by tides whose frequencies are well known (Hsieh et al., 1987; Xue et al., 2016; Rau et al., 2020; Schweizer et al., 2021).The moving average acts like a high-pass filter and the extraction of the tidal components at specific frequencies means that lower frequency and episodic events (atmospheric pressure changes related to weather systems passing across a site, rainfall and recharge events, and recession
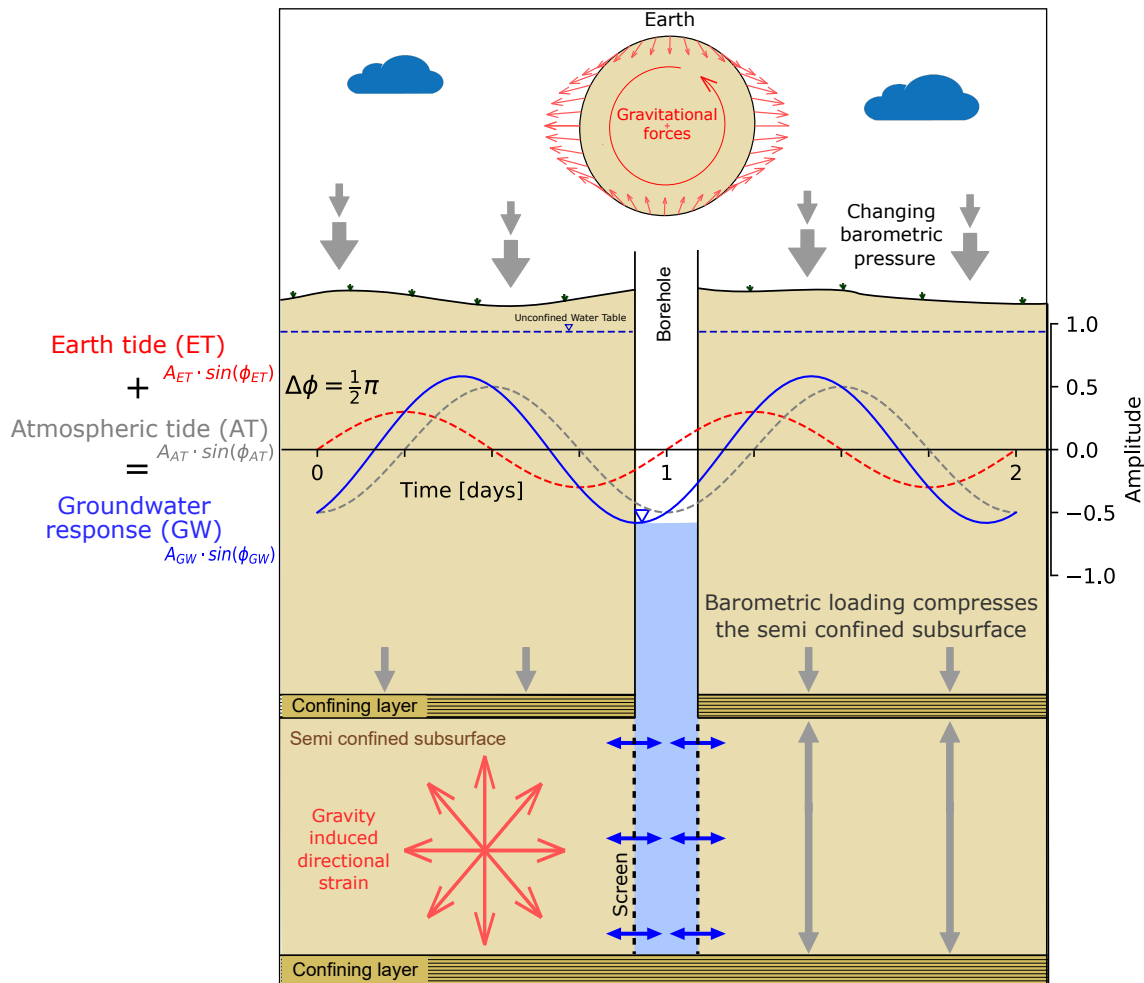
Figure 1. Representation of ~~the~~ groundwater level measured as pressure head ~~measured~~ in a well penetrating a confined aquifer with a ~~relatively~~ rigid matrix subjected to ET (red) and AT (grey), adapted from (McMillan et al., 2019). The result of these two effects can be expressed as a function of harmonic addition within the measured groundwater ~~level~~levels. ~~Here, the~~ The gravity-induced directional strain and vertical barometric loading ~~/unloading~~ combine to force water into and out of the well.

75 from pumping or droughts) present in the groundwater level/pressure data are discarded and therefore of no consequence for the analysis. Further, since our analysis is exclusively valid for the semi-confined and confined subsurface, water movement in the overlying shallow vadose zone and unconfined saturated zone is irrelevant. The extracted frequency components are complex numbers at discrete frequencies ($\hat{z}_{(f)}$, e.g. $\hat{z}_{M_2}$) for which amplitudes and phases can be calculated using the real and imaginary parts. The approach we use in our work (e.g. HALS) was comprehensively tested showing that it leads to accurate

80 estimates of harmonics in the presence of noise levels not exceeding the measurement resolution (Schweizer et al., 2021). High quality pressure transducers generally fulfil this criteria (Rau et al., 2019).

2.2 Earth tide influences on well water levels

2.2.1 Subsurface strain response to gravity changes

Rojstaczer and Agnew (1989) argued that for Earth tides horizontal areal strain is a sufficient approximation for depths of

85 up to thousands of kilometres. This approximation is therefore sufficient for application to groundwater resources as they are generally much shallower. The strain is often referred to as dilatation which is the total increase in volume of the material due to forcing by the Earth tides (in this case the tidal pull). In porous media, assuming incompressible grains, this dilatation is manifesting as an opening of the total pore space, decreasing the water pressure within the material (Agnew, 2010).

In this paper, we focus on the ET component at the frequency of 1.932274 (cpd) cycles per day (denoted by a subscript

90 of its Darwin name M_2) and the combined ET and AT component at the frequency of 2 cpd (denoted by a subscript of its Darwin name S_2), described in Table 1. While other frequency components can also be used (Hsieh et al., 1988; Merritt, 2004; Cutillo and Bredehoeft, 2011), M_2 and S_2 generally have the strongest tidal impact and their forces remains constant over time (Acworth et al., 2016; McMillan et al., 2019).

In this paper the term 'dilatation' is used broadly to represent both the dilation and compression due to the cyclical forcing

95 of the tides, consistent with its previous literature use (Xue et al., 2016; Allègre et al., 2016). The distortions by dilatation can be estimated through the planar strain concept known as tidal dilatation (Schulze et al., 2000; Fuentes-Arreazola et al., 2018). Tidal dilatation can be defined as

$$e = \frac{V}{g} \cdot \frac{e^v - 3e^h}{R}, \tag{1}$$

where V is the tidal potential (m^2/s^2), M_2 is the tidal frequency, g is acceleration due to gravity ($\approx 9.81 m/s^2$), e^v is vertical

100 displacement (-), e^h is horizontal displacement (-) (Agnew, 2010), R the average radius of the Earth (m) adjusted for any significant elevation and V is the tidal potential ($m^2 s^{-2}$) as defined in Table 1. The term ($e^v - 3e^h$) may also be approximated by Love-Shida numbers where e^v can be replaced by $\frac{L}{S}h$ with an assumed value of 0.6032 and e^h may be replaced with $\frac{L}{S}l$ with an assumed value of 0.0839 (Agnew, 2010; Cutillo and Bredehoeft, 2011). Previous work has demonstrated the use of theoretical Earth tides when analysing the groundwater response (Roeloffs, 1996; Xue et al., 2016; Allègre et al., 2016;

105 McMillan et al., 2019). The terms e^v and e^h can be directly calculated from software that generates theoretical Earth tide potential (ET^{pot}) or tidal dilatation (e) or tidal strains (ET^ϵ) based on geo-location, for example *ETERNA* (Wenzel, 1996),

TSoft (Van Camp and Vauterin, 2005), or, as was done for this paper, using *PyGTide* (Rau, 2018)~~(. This is~~ based on ETERNA ~~)~~and uses the *Wahr-Dehant-Zschau* model which assumes an elliptical, rotating, inelastic and oceanless Earth (Wahr, 1981; **?**).

The first approach using ET to estimate specific storage, used the potential for water movement from the tides to the corresponding water movement in a monitoring well in a confined aquifer for undrained conditions. Here, Bredehoeft (1967) defined specific storage (S_s) for a medium that is presumed to be incompressible as

$$S_s = - \left[\left(\frac{1-2v}{1-v} \frac{1-2\nu}{1-\nu} \right) \left(\frac{2_S^L h - 6_S^L l}{R \cdot g} \frac{2h_S^L - 6l_S^L}{R \cdot g} \right) \right] \frac{\Delta A_{M_2}^{ET^{pot}}}{\Delta h}, \tag{2}$$

where ν is the Poisson's ratio (generally assumed), h_S^L and l_S^L are dimensionless parameters describing earth properties (*Love-Shida* numbers), and $\Delta A_{M_2}^{ET^{pot}}$ is the change in the tidal potential to the corresponding change in hydraulic head Δh~~and v is typically an assumed Poisson's ratio~~. Here, the tidal dilatation (Equation 1), has been incorporated into Equation 2. Equation 2 was then used by Cutillo and Bredehoeft (2011) for is advantages over methods such as those provided by Hsieh et al. (1987), as it does not require the separation of individual tidal components, or the knowledge of a well's dimensions. Progressive improvements in the precision and duration of gravity measurement methods have since allowed for more accurate decomposition and cataloguing of the various tidal components (Agnew, 2010). These established catalogues of precise frequencies provide the basis for component separation using harmonic filtering techniques. The full separation of ET and AT at one frequency allows their individual and combined use towards better in-situ hydrogeomechanical characterisation (Rau et al., 2020).

We note that these ~~programs~~ codes do not account for ocean tide loading, i.e., the deformation of the subsurface due to the weight of the ocean tides. Ocean tide loading causes harmonic subsurface strain that is added to that imposed by Earth tides. The actual subsurface strain amplitude variation depends on the phase of both signals and is, in the worst cases, either added to or subtracted from the Earth tide. To understand the potential impact of this effect we used the ocean tide loading provider by Chalmers University of Technology (http://holt.oso.chalmers.se/loading/index.html) to estimate the M_2 aerial strain amplitude for our five locations with the state-of-the-art finite element model FES2014b (Penna et al., 2008; Matviichuk et al., 2021). However, we further note that ocean tide loading is a complicated phenomenon (Jentzsch, 1997) and its detailed assessment is beyond the scope of this manuscript.

2.2.2 Well water level response to harmonically forced pore pressure

The relative amplitude response of the groundwater, as measured in a borehole in relation to the tidal dilatation or strain can be expressed as (Hsieh et al., 1987; Xue et al., 2016; Allègre et al., 2016)

$$A_{M_2}^{ET^\epsilon} = \left| \frac{\hat{z}_{M_2}^{GW}}{\hat{z}_{M_2}^{ET^\epsilon}} \right| = \frac{A_{M_2}^{GW}}{A_{M_2}^{ET^\epsilon}}, \tag{3}$$

where $\hat{z}_{M_2}^{GW}$ and $\hat{z}_{M_2}^{ET^\epsilon}$ are the complex frequency component of the groundwater pressure head and tidal strain, respectively; $A_{M_2}^{GW}$ is the amplitude of the groundwater pressure head fluctuation and $A_{M_2}^\epsilon$ is the amplitude of the tidal strain fluctuation, all at the frequency of the M_2 tidal component. Note that $A_{M_2}^{ET^\epsilon}$ is also referred to as areal strain sensitivity (Hsieh et al., 1987).

It is important to note the difference presented in Equation 3 from Xue et al. (2016) with the original dimensionless amplitude response calculated by Hsieh et al. (1987) as

$$A_{M_2} = \left| \frac{\hat{z}^{GW}_{M_2}}{\hat{z}^{p}_{M_2}} \right| = A^{ET^\epsilon}_{M_2} S_s, \tag{4}$$

where $\hat{z}^{p}_{M_2}$ is the complex aquifer pore pressure response (superscript p reflects pore). Here, the denominator term has changed from the complex amplitude of the pressure fluctuation to the tidal dilatation, effectively incorporating Equation 2. This key difference allows for the addition of the storage term S_s within the amplitude response equations due to the sensitivity of storage to the amplitude response for confined and leaky responses described in Sections 2.2.3 and 2.2.4. A_{M_2} from Equation 4 is dimensionless, with values $0 \leq A_{M_2} \leq 1$.

The phase shift (or phase difference) is defined as the strain response observed as the complex groundwater pressure head (water level) fluctuation, minus the phase of the complex tidal dilatation (tidal forcing) stress, defined as

$$\Delta\phi_{M_2} = \arg\left(\frac{\hat{z}^{GW}_{M_2}}{\hat{z}^{ET^\epsilon}_{M_2}} \right) = \phi^{GW}_{M_2} - \phi^{ET^\epsilon}_{M_2}, \tag{5}$$

where $\phi^{GW}_{M_2}$ is the phase angle expressed in the groundwater response and $\phi^{ET^\epsilon}_{M_2}$ is the phase angle of the theoretical Earth tide component, in this case at the frequency of the M_2. A negative phase shift is expressed where the groundwater response lags behind the induced strain (i.e., water level response lags behind the pressure head disturbance (Hsieh et al., 1987)), whereas a positive phase shift indicates the groundwater response is leading the strain response.

It should be noted that in this method development, a homogeneous, isotropic aquifer of infinite lateral extent is assumed for all derivations (Hsieh et al., 1987). All derived hydro-geomechanical variables are treated as bulk properties averaged over a distinct but unknown volume, representative of the EAT area of influence around the monitoring wells screened interval, including effects from geological heterogeneities and the well construction, such as the inclusion of a gravel pack. The exact nature and dimensions of the volume of influence, i.e., the volume of sub-surface around the well being 'sampled' is currently unresolved. It is commonly assumed that the ET amplitude response is negligibly influenced by fluid flow when the screened aquifer is confined (Xue et al., 2016). Instead, it is predominantly controlled by a change in storage. This is used as a justification to modify the hydraulic diffusivity term in the amplitude response equations to $1/Ss$ when including the Earth tide strain estimation (Equations 6 and 13), i.e. the tidal dilatation (Hsieh et al., 1987; Wang, 2000; Xue et al., 2016).

2.2.3 Confined water level response

Positive and negative phase shifts are either leading (leaky) or lagging (confined), respectively, in relation to the strain response expressed by the water level in a well to formation tidal forcing. Hsieh et al. (1987) provided an analytical solution for the confined groundwater flow equation with harmonic forcing to describe the relationship between aquifer pore pressure and well water level. Their model assumes horizontal flow only and is formulated in terms of amplitude ratio and phase shift, thereby allowing for the solution of two properties, transmissivity and storativity from the amplitude and phase response. The confined

(negative phase) model is defined by Hsieh et al. (1988) as

$$A_{M_2} = \frac{1}{\sqrt{(E^2 + F^2)}} \tag{6}$$

and

$$\Delta\phi_{M_2} = -\tan^{-1}\left(\frac{F}{E}\right) \tag{7}$$

~~where~~ with the following parameters

$$E = 1 - \frac{\omega r_c^2}{2T}[\Psi Ker(\alpha_w) + \psi Kei(\alpha_w)] \frac{\omega r_c^2}{2T}\left[\Psi Ker(\alpha_w) + \psi Kei(\alpha_w)\right] \tag{8}$$

and

$$F = \frac{\omega r_c^2}{2T}[\psi Ker(\alpha_w) - \Psi Kei(\alpha_w)] \frac{\omega r_c^2}{2T}\left[\psi Ker(\alpha_w) - \Psi Kei(\alpha_w)\right]. \tag{9}$$

~~and~~ These include

$$\Psi = \frac{-[Ker_1(\alpha_w) - Kei_1(\alpha_w)]}{2^{\frac{1}{2}}\alpha_w[Ker_1^2(\alpha_w) + Kei_1^2(\alpha_w)]} \frac{-[Ker_1(\alpha_w) - Kei_1(\alpha_w)]}{\sqrt{2}[Ker_1^2(\alpha_w) + Kei_1^2(\alpha_w)]\alpha_w} \tag{10}$$

and

$$\psi = \frac{-[Ker_1(\alpha_w) + Kei_1(\alpha_w)]}{2^{\frac{1}{2}}\alpha_w[Ker_1^2(\alpha_w) + Kei_1^2(\alpha_w)]} \frac{-[Ker_1(\alpha_w) + Kei_1(\alpha_w)]}{\sqrt{2}[Ker_1^2(\alpha_w) + Kei_1^2(\alpha_w)]\alpha_w}, \tag{11}$$

where

$$\alpha_w = r_w\sqrt{\frac{\omega S}{T}} = r_w\sqrt{\frac{\omega}{D_h}}. \tag{12}$$

Here, Ker, Kei and Ker_1, Kei_1 are the real and imaginary parts of the Kelvin function of order zero and one, respectively. The storativity S and transmissivity T can be related to specific storage as $S = S_s b$ and hydraulic conductivity as $T = k^f b$, respectively; b is the aquifer thickness, which when the aquifer thickness is unknown is approximated with the vertical screen length; r_w is the internal radius of the well screen (accounts for well storage); r_c is the outer radius of the casing. Ker and Kei are Kelvin functions of zero order, and Ker_1 and Kei_1 are Kelvin functions of the first order. Figure 2a,b show the amplitude and phase solution space when considering the strain response as well as separation of hydraulic properties, respectively.

2.2.4 Leaky water level response

The leaky water level model is based on the description of a periodic load on a half-space, as described by Wang (2000), and is used for Earth tides where a vertical pressure propagation and flow exist (Xue et al., 2016; Allègre et al., 2016). The Equations 13 and 14 were derived from the force equilibrium equations (refer to Wang (2000))

$$A_{M_2} = \sqrt{1 - 2\exp\left(-\frac{z}{\delta}\right)\cos\left(\frac{z}{\delta}\right) + \exp\left(-2\frac{z}{\delta}\right)}, \tag{13}$$
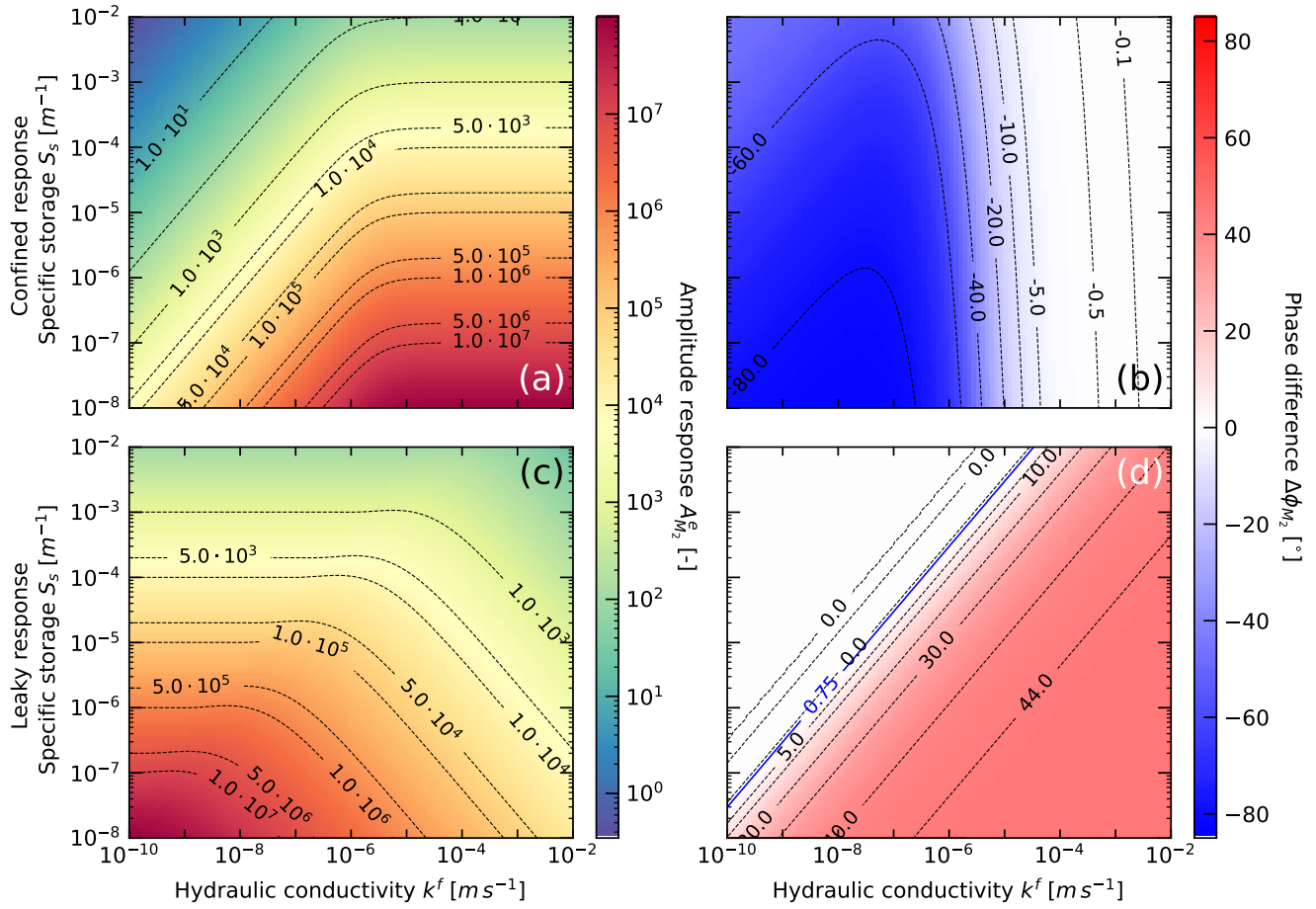
Figure 2. Pressure head amplitude and phase response to the Earth tide M_2 component as a function of ranges in hydraulic conductivity and specific storage: (a) ~~amplitude~~ Amplitude response (Equation 6) and (b) phase shift (Equation 7) ~~response~~ for confined conditions (~~here;~~ the radius of borehole and screen are 0.1 m and the screen length is 2 m). (c) ~~amplitude~~ Amplitude response (Equation 13) and (d) phase shift (Equation 14) ~~response~~ for semi-confined conditions ~~where~~ with vertical flow ~~may exist~~ (the depth of the screen is ~~set to~~ 20 m).

and

$$\Delta\phi_{M_2} = \tan^{-1}\left[\frac{\exp\left(-\frac{z}{\delta}\right)\sin\left(\frac{z}{\delta}\right)}{1 - \exp\left(-\frac{z}{\delta}\right)\cos\left(\frac{z}{\delta}\right)}\right], \tag{14}$$

195 where z is depth of the midpoint open screen interval, ω is the angular frequency of the tidal component (M_2),

$$]\frac{2D_h}{\omega},$$

$$-$$

200

$$]\frac{2D_h}{\omega}.$$

(15)

Here, D_h is then the hydraulic diffusivity, defined as

205 $$D_h = \frac{T}{S} = \frac{k^f}{S_s} = \frac{k}{\mu S} = \frac{\rho_w g k^f}{\mu S_s^p} \frac{\rho_w g k^f}{\mu S_s},$$ (16)

where T is ~~subsurface~~ the transmissivity ($T = k^f b$), k is permeability, k^f is hydraulic conductivity, ρ_w is the density of water (0.9982 kg/L at $20°C$) and μ is the dynamic viscosity of water ($8.90 \cdot 10^{-4}$ Pa s), S is storativity ~~and S_s^p is specific storage (1/Pa)~~. Equations 13 and 14 require iterative solving for D_h and S_s.

Figure 3 shows the solution space for Equations 13 and 14. It is noteworthy that the amplitude can be attenuated significantly

210 for high hydraulic diffusivities and shallow depths. Overall, confined conditions should prevail for low hydraulic diffusivities and larger depths where the amplitude ratio is ≈ 1. Semi-confined conditions are indicated by positive phase shifts. Note that hydraulic diffusivities in the range of 0.01 to 0.1 ($m^2 s$) can increase the amplitudes to approx. 1.07 (Figure 3a) for which phase shifts can assume negative values (e.g., ~~$-0.5°C$~~ $-0.5°$ in Figure 3b). Figure 2c,d show the solution space when considering the strain response as well as separation of hydraulic properties for leaky conditions.

215 **2.2.5 Distinguishing between leaky and confined conditions**

The sets of Equations 6 and 7 (Hsieh et al., 1987) describe lateral water movement between the well-bore and surrounding subsurface, whereas Equations 13 and 14 (Wang, 2000) explain the positive phase shift by allowing vertical flow within the groundwater system. Both sets of equations have been used to estimate hydraulic conductivity and specific storage. This is achieved by decomposing the hydraulic diffusivity using the assumptions outlined at the end of Section 2.2.2.

220 The phase shift determines which of these sets of analytical solutions are appropriate. For a phase shifts $-45° \leq \Delta\Phi_{M_2} < 0°$ the confined response model is used, and for a phase shifts between $0 \leq \Delta\Phi_{M_2} \leq 90°$ the leaky response model is applied (both are visualised in Figure 2). Note that the leaky model may result in a slight negative phase shift for certain parameter ranges. Consequently, there is a range of ambiguity in phase shift values between $-1°$ to $0°$ in which both sets of solutions should be used, and the most physically plausible results should be selected (Xue et al., 2016). Note, the unit input as either pressure or

225 hydraulic head will also be carried through the equations resulting in a unit difference where S_s^p is specific storage expressed in $1/Pa$ whereas S_s is specific storage expressed as $1/m$, as demonstrated in Equation 16.
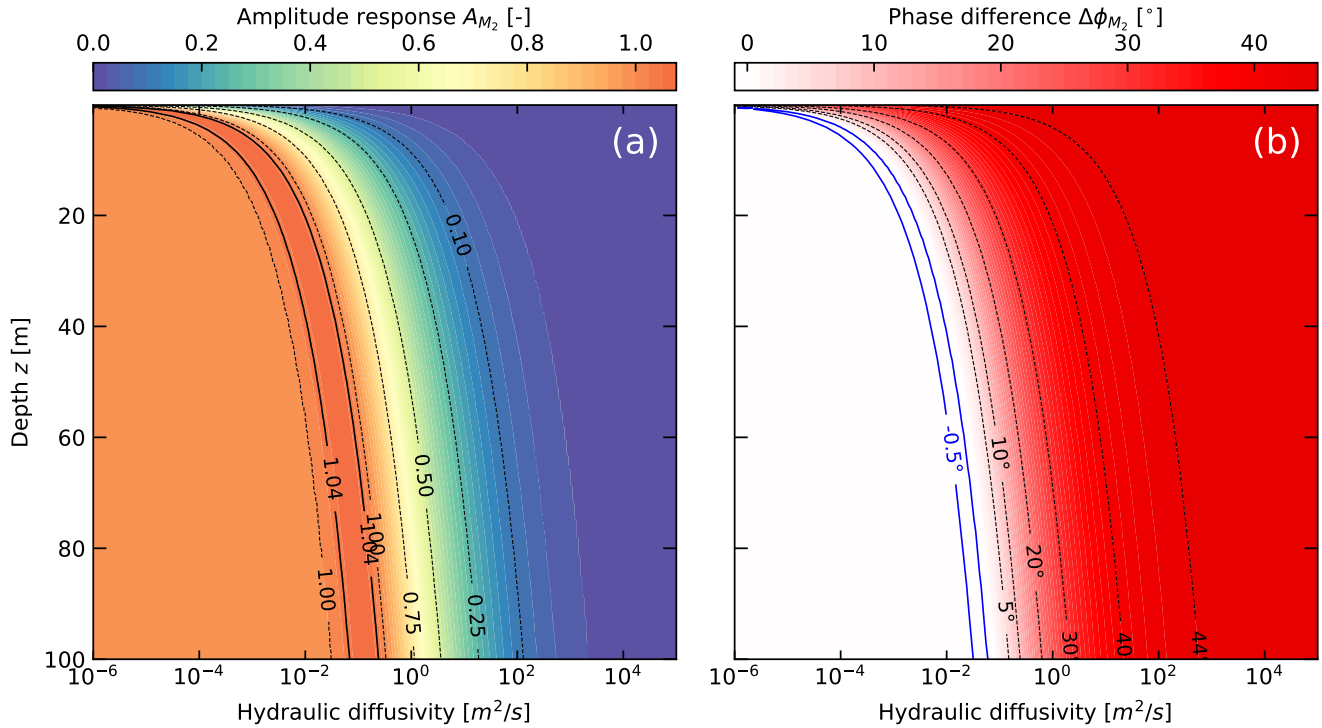
Figure 3. Periodic loading of a half space (applied to ET) as ~~modelled~~ represented by Equations 13 and 14. (a) Normalised ~~relative~~ amplitude response ~~and hydraulic diffusivity~~ as a function of hydraulic diffusivity and depth (Equation 13). (b) Phase response ~~and hydraulic diffusivity~~ as a function of depth and hydraulic diffusivity (Equation 14) (Wang, 2000).

2.3 Atmospheric tide influences on well water levels

Methods that quantify the barometric efficiency of subsurface systems are based on quantifying the groundwater response magnitude to atmospheric pressure changes (Clark, 1967; Rasmussen and Crawford, 1997; Barr et al., 2000; Gonthier, 2003) or atmospheric tides (Acworth et al., 2016). Turnadge et al. (2019) reviewed these methods and concluded that the method by Acworth et al. (2016) was the most robust and reliable. However, their approach was limited by the assumption of an instantaneous and undamped response. Rau et al. (2020) developed a new method that completely disentangles the influences of Earth and atmospheric tides at the same frequency, e.g. S_2. This further considers the damping of the amplitude that can be caused by low hydraulic conductivity materials under confined conditions (Section 2.2.3) or attenuation of the amplitude under semi-confined conditions (Section 2.2.4). Their new approach is (Rau et al., 2020)

$$BE_{S_2} = \frac{1}{A_{M_2}} \cdot \left| \frac{\hat{z}_{S_2}^{GW.AT}}{\hat{z}_{S_2}^{AT}} \right|, \tag{17}$$

where

$$\hat{z}_{S_2}^{GW.AT} = \hat{z}_{S_2}^{GW} - \hat{z}_{S_2}^{GW.ET} = \hat{z}_{S_2}^{GW} - \frac{\hat{z}_{M_2}^{GW}}{\hat{z}_{M_2}^{ET}} \hat{z}_{S_2}^{ET}. \tag{18}$$

Here, A_{M_2} corrects for the damping of the subsurface-well system and can be inferred from Earth tides (Equation 4) for confined conditions, e.g. for low hydraulic conductivity (Equation 6), or damping under semi-confined conditions (Equation 13). $\hat{z}_{S_2}^{GW.AT}$ is the S_2 component of the groundwater response to atmospheric tides, and $\hat{z}_{S_2}^{AT}$ is the S_2 frequency component (atmospheric tide) embedded in atmospheric pressure measurements. BE forms a stress balance, described as (Jacob, 1940)

$$BE + \gamma = 1, \tag{19}$$

where γ is the loading efficiency.

2.4 Combining Earth and atmospheric tide responses

2.4.1 General relationships

Within the following derivations it is assumed that Earth tides only induce horizontal areal strain ($\epsilon_x y = \epsilon_x + \epsilon_y$) whereas atmospheric tides only induce vertical strain ($\epsilon_z = -p^{AT}$) (Rojstaczer and Agnew, 1989; Cutillo and Bredehoeft, 2011), all of which are assumed to act instantaneously on the subsurface as is consistent with previous literature (Wang, 2000; Rau et al., 2018). Under such conditions, van der Kamp and Gale (1983) has shown that the rigidity modulus (also known as the shear modulus, G) can be estimated, with the previous outlined assumptions, from combined Earth and atmospheric tide influences as

$$G = A_{M_2}^{ET^\epsilon} \frac{\rho g}{2\gamma} = A_{M_2}^{ET^\epsilon} \frac{\rho g}{2(1 - BE)}, \tag{20}$$

where, $A_{M_2}^{ET^\epsilon}$ originates from Earth tides (Equation 3), whereas BE or γ is derived from atmospheric tides (Equation 19).

The disentanglement of Earth and atmospheric tides from the groundwater level response in a well, and the subsequent use of these separate frequency components to quantify hydrogeomechanical properties allows further geomechanical derivations to be made. Two methods are presented below which solve for the assumption of either incompressible (suitable for unconsolidated material) or compressible grains (suitable for consolidated material). The choice between which method to use is established by examining an estimated *Biot-Willis* coefficient defined as (Wang, 2000)

$$\alpha = 1 - \frac{K}{K_s} = 1 - \frac{\beta_s}{\beta}. \tag{21}$$

Where K is the Bulk modulus, K_s is the Bulk modulus of the solid grain, β is the compressibility, and β_s the compressibility of the solid grain. For unconsolidated conditions, where the Bulk modulus is much smaller than the Bulk modulus of the grains ($K \ll K_s$) it is possible to assume that the grains do not contribute to the overall compressibility, thus the grains are incompressible. The *Biot-Willis* coefficient $\alpha \to 1$ shows that the contribution of the grains to the compressibility of the bulk material is insignificant (Rau et al., 2018). By contrast, in consolidated cases K becomes larger, leading to a coefficient that

deviates appreciably from one ($\alpha < 1$). In such cases, the grain compressibility is a significant proportion of the total material compressibility and must be accounted for.

2.4.2 Unconsolidated systems

In unconsolidated systems, the compressibility of the grains is much smaller than that of the bulk leading to $\alpha = 1$. This allows simplification of the theory. In the following, undrained parameters are indicated by the superscript u. The uniaxial loading efficiency is related to the uniaxial bulk properties as (van der Kamp and Gale, 1983)

$$\gamma = \frac{\beta_v^u}{\theta \beta_f + \beta_v^u}, \tag{22}$$

where β_f is the compressibility of the fluid ($4.59 \times 10^{-10}\ Pa^{-1}$ at $20°C$), β_v^u is the vertical undrained bulk compressibility and θ is the total porosity of the formation. The uniaxial specific storage (assuming incompressible grains) is defined by Jacob (1940) as

$$S_s = \rho_w g (\beta_v^u + \theta \beta_f). \tag{23}$$

Acworth et al. (2016) used Equation 22 to simplify Equation 23 as follows

$$S_s = \rho_w g \beta_f \frac{\theta}{BE} = 4.5 \times 10^{-6} \frac{\theta}{BE}. \tag{24}$$

However, this requires a prior estimate of the porosity θ which is often difficult to determine due to the lack of independent measurements.

Note that the above equations assume that barometric loading is uniaxial, and as such use vertical compressibility (β_v^u) rather than the volumetric (bulk) compressibility (β^u). Here, were instead propose using the S_s derived from the response to ET (Section 2.2) to instead estimate the subsurface porosity by rearranging Equation 24 (similar to Jacob (1940)) as

$$\theta = \frac{S_s BE}{\rho_w g \beta_f} = \frac{S_s}{\rho_w g \beta_f}(1 - \gamma). \tag{25}$$

To achieve a similar outcome as Acworth et al. (2016) this porosity, in addition to the calculated S_s, can also be used to provide a uniaxial (vertical) bulk compressibility (inverse vertical undrained bulk modulus (K_v^u)) of the subsurface defined as (Acworth et al., 2016)

$$\beta_v^u = \frac{1}{K_v^u} = \theta \beta_f \frac{\gamma}{1 - \gamma}. \tag{26}$$

This approach is similar to Cutillo and Bredehoeft (2011) but uses the objective BE method developed by Rau et al. (2020) instead of the subjective correlation by Gonthier (2003). Within this subsection it has been shown that it is possible to derive an estimate of porosity from a loading strain if the specific storage is known. This assumes incompressible grains ($\alpha \approx 1$) and is therefore applicable for unconsolidated materials (Rau et al., 2019).

The assumption of incompressible grains allows for the removal of the grain compressibility and provides a simplification of the poroelastic parameter space. This step combined with the new derivation of the shear modulus enables a linear analytical

solution of the remaining elastic variables in unconsolidated material ($\alpha \approx 1$). The first step can be taken by deriving the undrained bulk modulus (K_u) with the K_v^u from Acworth et al. (2016) as (Wang, 2000)

$$K^u = K_v^u - \frac{4}{3}G, \tag{27}$$

which allows solving the Skempton coefficient defined as (Rau et al., 2018)

$$B = \gamma \frac{K_v^u}{K^u} = \gamma \frac{\beta^u}{\beta_v^u}. \tag{28}$$

Determination of the Skempton coefficient along with the loading efficiency unlocks the undrained Poisson's ratio using (Wang, 2000)

$$\nu^u = \frac{3\gamma - B}{3\gamma + B} \tag{29}$$

and drained Poisson's ratio as (Wang, 2000)

$$\nu = \frac{3\nu^u - B(1 + \nu^u)}{3 - 2B(1 + \nu^u)}. \tag{30}$$

Determination of the drained Poisson ratio further unlocks all remaining poroelastic properties such as Young's Modulus (E), defined as (Wang, 2000)

$$E = \frac{9KG}{3K + G}. \tag{31}$$

Equations 22-31 define the complete parameter space for unconsolidated materials.

2.4.3 Consolidated systems

To determine the poroelastic properties of consolidated materials, the grain compressibility must be considered leading to $\alpha < 1$. Further, the following two assumptions must be made: (1) Although pore fluids technically respond to cubic strains, the areal strain can be used to estimate the subsurface strain from ET; (2) The system is homogeneous and laterally extensive, thus ignoring topographic effects and considering the barometric loading to be uniform. The equations that define the remaining elastic properties for such conditions are (Beavan et al., 1991) Skempton's constant

$$B = \frac{3\gamma(1 - \nu)}{2\gamma\alpha(1 - 2\nu) + (1 + \nu)}, \tag{32}$$

and

the total porosity

$$\theta = \left(\frac{1}{B} - 1\right)\left(\frac{1}{K} - \frac{1}{K_s}\right)\left(\frac{1}{k^f} - \frac{1}{K_s}\right)^{-1}, \tag{33}$$

and

320 the Biot-Willis coefficient

$$\alpha = 1 - \frac{K}{K_s} = 1 - \frac{2G(1+\nu)}{3K_s(1-2\nu)} \tag{34}$$

and

and the specific storage

$$S_s = \frac{\rho g}{\gamma(1-\nu)}\left(\frac{1-2\nu}{2G} - \frac{1+\nu}{3K_s}\right). \tag{35}$$

325 Equations 32-35 form a non-linear system which must be solved by iteration.

If the petrology of the lithology is known, appropriate literature compressibility values of the dominant grain mineralogy (K_s) could be used. Quartz is the most common naturally occurring mineral and is also one of the least compressible (it is also applicable for most of our case sites), and it will therefore be used to define the upper bounds of K_s here. Richardson et al. (2002) summarised literature values of poly-crystalline quartz for K_s to range between 36-40 GPa, and reported K_s values for 330 the quartz Ottawa Sandstone to be in a range of 30-50 GPa. The average of these ranges has been summarised as 42 GPa (Rau et al., 2018) and will be used in this work.

With the established inputs of $\gamma(BE)$, A_{M_2}, G (Equation 20), S_s and an estimate of K_s, it is possible to simultaneously solve Equations 32-35 for Skempton's coefficient (B), porosity (θ), *Biot-Willis* coefficient (α) (Beavan et al., 1991). This allows a complete calculation of all remaining poroelastic properties using the relationships that can be found in (Wang, 2000).

335

3 Examples of method applications

3.1 Field sites, datasets and interpretation

To demonstrate the new method, groundwater and barometric pressure records from four field sites and five monitoring bores were used. These sites were selected based on three main criteria: (1) Data availability and quality; (2) a significant ground- 340 water response to Earth tides (M_2); (3) providing a variety of hydrogeological settings with existing studies for parameter comparisons. Further details about each site is described in separate sections below. Specific bore geometries and measurements used in the analysis of these sites such as depths and bore construction, such as casing and screen radius's, screen depth and length, are summarised in Table 2.

Groundwater pressure head and barometric pressure time-series were recorded at sub-hourly intervals at all sites (e.g. two 345 sites shown in Figure 4) for at least three months which is longer than the $\sim$28 days being suggested as the minimum requirement of the HALS method used here (Schweizer et al., 2021). Geo-position of the boreholes, theoretical Earth tide strain for the same duration and sampling frequency of each site as well as aerial strain amplitudes from ocean tide loading for M_2 are summarised in Table 2.

Location	Borehole	Geolocation			Inputs					Description
		Latitude	Longitude	Height	r_c	r_w	b	z	K_s	Lithology
Cattle Lane	BH30061	-31.518340	150.468332	313	*0.125*	*0.12*	*1*	55	∞	Sand, Gravel, Clay
Thirlmere	GW075409.1.2	-34.230666	150.543996	314	*0.156*	*0.14*	*12*	78	∞	Quartz arenite sandstone
Thirlmere	Thirlmere 2	-34.220836	150.53646	323	0.114	0.108	4	72	42	Quartz arenite sandstone
Dodowa	BH11	5.881675	0.097244	88	0.058	0.048	2	45	42	Gneiss
Death Valley	BLM-1	36.408130	-116.471360	688	0.127	0.127	106	*830*	42	Carbonate

Table 2. Inputs parameters for case sites where; r_c is the outer diameter (m) of the bore casing, r_w the internal diameter (m) of the bore casing, b is the Aquifer thickness (m) or open interval of the screen, z is the depth (m) to the centre of the screen or open bore interval, and K_s is the assumed grain bulk modulus. Italicised values were not used in the applied leaky or confined models, but are provided for completeness and context.

Borehole	Hydraulic results							
	$A_{M_2}^{ET^\epsilon}$	$A_{M_2}^{OT^\epsilon}$	$A_{M_2}^\epsilon$	A_{M_2}	$\Delta\Phi_{M_2}$	$<K>$	S_s	BE
BH30061	20.62	2.48	$4.59 \cdot 10^4$	0.765	24.89	$5.4 \cdot 10^{-6}$	$1.7 \cdot 10^{-5}$	0.11
GW075409.1.2	19.36	3.81	$3.24 \cdot 10^5$	1.039	10.05	$4.8 \cdot 10^{-7}$	$3.2 \cdot 10^{-6}$	0.38
Thirlmere 2	19.07	3.81	$3.52 \cdot 10^5$	0.988	-4.74	$1.9 \cdot 10^{-5}$	$2.8 \cdot 10^{-6}$	0.35
BH11	27.57	4.10	$1.31 \cdot 10^6$	0.948	-13.80	$2.6 \cdot 10^{-6}$	$7.2 \cdot 10^{-7}$	0.70
BLM-1	17.55	2.52	$1.49 \cdot 10^6$	0.998	-1.07	$4.3 \cdot 10^{-6}$	$6.7 \cdot 10^{-7}$	0.62

Table 3. Hydraulic results where $A_{M_2}^{ET^\epsilon}$ is the Earth tide nano-strain amplitude (nstr), $A_{M_2}^{OT^\epsilon}$ is the ocean tide strain amplitude (nstr), $A_{M_2}^\epsilon$ is the strain response amplitude (m/nstr), A_{M_2} is the amplitude ratio (-), $\Delta\Phi_{M_2}$ is the phase shift (degrees), $<K>$ is hydraulic conductivity (m/s), S_s is the specific storage (1/m), BE is the barometric efficiency (-).

All time-series were detrended by fitting a linear function through a moving 3-day window using the *SciPy* detrend func-
tion, and the main tidal components were extracted using *HALS* (Section 2.1). Tables 3 and 4 contain the estimated hydro-
geomechanical properties for all the field sites and are discussed in the sections below.

In this paper, all of the methodology and equations were implemented in the *Python* programming language, and joint
iterative solving was completed using *SciPy*'s least-squares functionality. The following realistic parameter bounds were con-
sidered during root finding: $0 \leq B \leq 1, -1 \leq \nu \leq 0.5, 0.005 \leq G \leq 40$ GPa, $0 \leq \theta \leq 0.5$. We note that (1) the parameter units
were scaled to avoid bias towards parameters with large values, (2) the solver was set to 64-bit machine precision (epsilon
$1.11 \cdot 10^{-16}$), (3) none of the estimated parameters reached or exceeded any of the prescribed solution constraints.

3.2 Cattle Lane (NSW, Australia)

Cattle Lane is located on the Liverpool Plains, NSW, eastern Australia. Erosion of the basaltic Liverpool Ranges to the south
produced a succession of unconsolidated silts, clays, sands, gravel and minor carbonate nodules within the Liverpool Plains. A
thick sequence of clay bound sediments overlie a gravel aquifer at 40 m. This aquifer has previously be shown to respond to
loading by rainfall events (Timms and Acworth, 2005). The lithology of the 1 m screened interval was described by Acworth
et al. (2015) as major basalt fragments mixed with coarse sand, shell and carbonate nodules. The site has previously been
cored to 31.5 m depth, lithologically logged and geophysical surveyed, confirming that it is horizontally extensive (Acworth
et al., 2015). Cross-hole seismics were also conducted by Rau et al. (2018) to the depth of 40 m (the screened interval of bore
BH30061 is at 55 m depth, see Table 2), providing depth profiles of seismically inferred elastic variables that were used to
constrain the pore pressure response to atmospheric tides analysis.

Further studies at this site include Acworth et al. (2016) and Acworth et al. (2017), which were precursors to Rau et al.
(2018) in the investigation of pore pressure response to atmospheric tides, and Timms et al. (2018) on a core scale analysis of
the site's laterally extensive and thick aquitard. Due to the sufficient M_2 response, time-series data of groundwater pressure

Borehole	Poroelastic results									
	θ	K_v^u	G	K^u	B	ν^u	ν	K	E	α
BH30061	0.39	3.8	0.3	3.5	1.0	0.46	-0.29	0.1	0.4	1
GW075409.1.2	0.27	9.7	2.6	6.3	1.0	0.32	-0.04	0.3	1.9	1
Thirlmere 2	0.19	16.6	2.6	13.1	0.9	0.38	-0.03	1.6	5.1	0.96
BH11	0.08	58.8	21.6	30.0	0.7	0.10	-0.21	8.1	34.2	0.81
BLM-1	0.06	64.2	19.1	38.7	0.8	0.16	-0.23	6.7	29.4	0.84

Table 4. Poroelastic results where θ is porosity (-), K_v^u is the vertical undrained bulk modulus, G is the shear modulus (GPa), K^u is the undrained bulk modulus, B is *Skempton*'s coefficient (-), ν^u is the undrained Poisson's Ratio (-), ν is Poisson's Ratio (-), K is Bulk Modulus (GPa), E is Young's modulus (GPa) and α is the *Biot-Willis* coefficient (-).

heads measured between the 21/01/2016 and 14/04/2018 were used from the bore BH30061. The groundwater pressure heads were collected using vented In-Situ Troll 700H series loggers at hourly intervals and sub-millimetre precision. Atmospheric pressure was measured by an In-Situ Baro Troll absolute gauge transducer.

The borehole BH30061 from Cattle Lane produced positive M_2 phase shifts (Table 2), with specific storage and hydraulic conductivity therefore being derived from the leaky model (Section 2.2.4). When applying the grain compressibility of quartz ($K = 42$ GPa) a *Biot-Willis* coefficient of 0.99 is obtained and hence justifies the assumption of incompressible grains ($\alpha \approx 1$) and the unconsolidated analytical model (Section 2.4.2).

The specific storage, hydraulic conductivity, porosity, shear modulus, and undrained Poisson's ratio from Cattle Lane are consistent with literature values for the sediment type (Bowles, 1996), and comply with previous estimates from higher in the stratigraphy at the same site obtained by cross-hole seismics (Acworth et al., 2015, 2016; Rau et al., 2018). The Young's modulus of 0.4 GPa deviates from the expected material range reported in the literature for an unconsolidated clay, sand and gravel mixture of between 0.025 and 0.2 GPa, although the obtained value is reasonable when considering the degree of consolidation at 55 m depth and the in-situ determination rather than those obtained from laboratory tests (Bouzalakos et al., 2016). The Poisson's Ratio of -0.29 is the only parameter that deviates significantly from the expected range of 0.2 to 0.5. This will be discussed later.

3.3 Thirlmere Lakes (NSW, Australia)

The Thirlmere Lakes are located in the south-west of the Sydney Basin, NSW. Both bores are located in the quartz arenite Hawkesbury sandstone, which is about 100 m thick at the site. This sandstone is deposited by a braided river with the heterogeneous deposits showing overlapping and self incised fining up sequences, with over-bank deposited fines at paleo-channel boundaries (Miall and Jones, 2003). There is evidence that the upper portion of bore Thirlmere 2 passes through a geological fault damage zone, with drilling fluid losses recorded above the screened interval due to fractures (Impax, 2019). Other studies

in the same lithology include Ross (2014), which investigated the potential for a bore field development within the Hawkesbury Sandstone, however, no publicly available studies exist for this lithology at the case site.
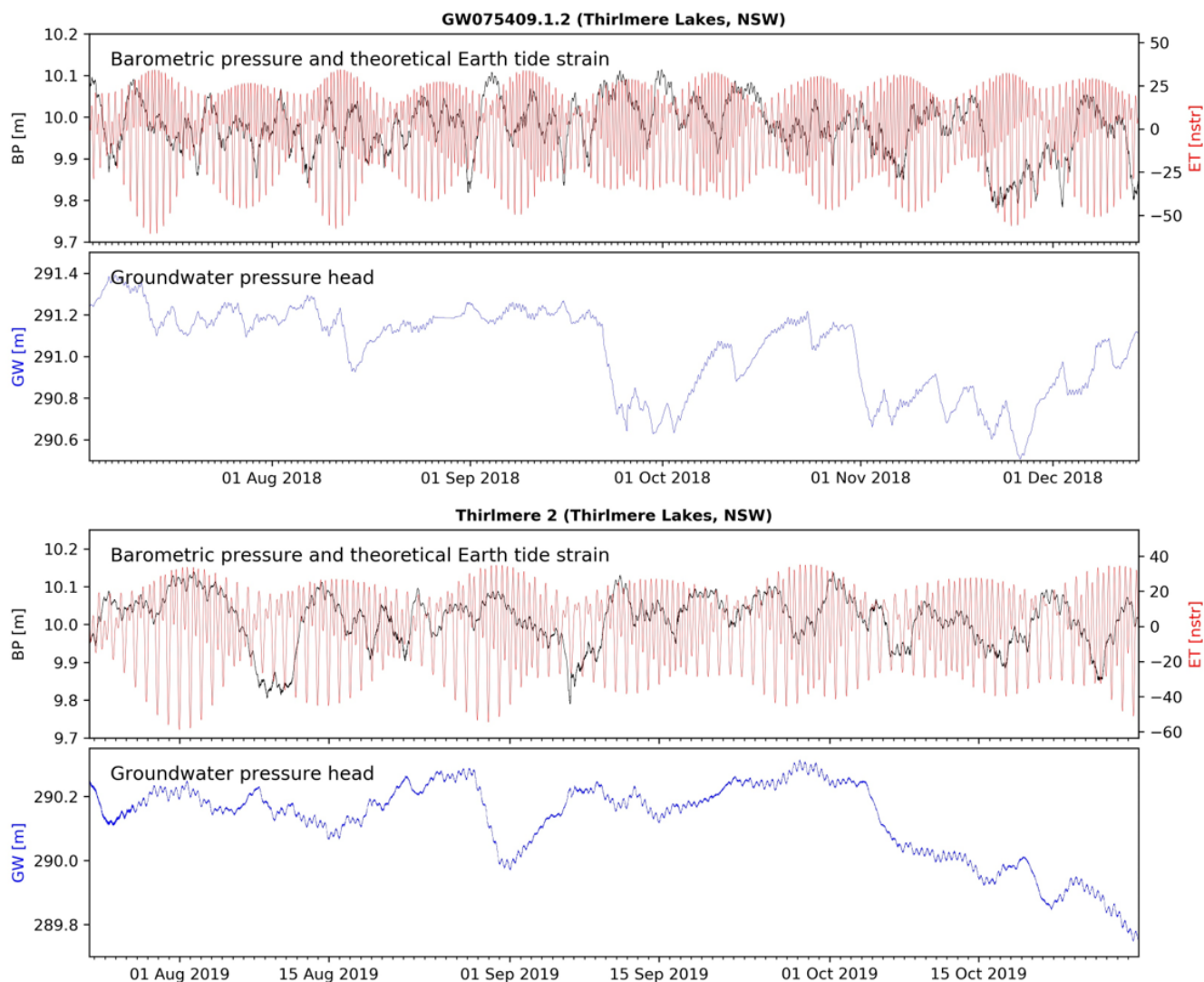
Figure 4. Time-series of ~~barometric pressures (m), theoretical Earth tide nano-strain (nstr) from *PyGTide* for the corresponding~~ groundwater levels from bores GW075409.1.2 and Thirlmere 2 ~~from~~ located at Thirlmere Lakes ~~,~~ (NSW, Australia), barometric pressures (in m equivalent water heights for easier comparison to the groundwater pressure heads), corresponding theoretical Earth tides (in nano-strain, nstr) calculated using *PyGTide*.

395   The time span and collection frequency of the time-series data for the two bores differ. The time-series for GW075409.1.2 (Russell, 2012) covers the time period from 03/07/2018 to 14/12/2018 and was downloaded from the *WaterNSW* real-time data portal with 15 min intervals. For this bore a coinciding barometric time-series data was obtained from a weather station

approx. 500 m away. The bore Thirlmere 2 is located about 2 km from GW075409.1.2 and geo-coordinates are shown in Table 2. The time-series data for Thirlmere 2 was collected for this study using a vented In-Situ Troll 700H series pressure transducer

400   every 5 min between the 32/07/2019 and 29/10/2019. The coinciding barometric time-series was collected using a Solinst Baro-logger installed in the airspace of the borehole. The field data is summarised in Figure 4 together with the theoretical Earth tide data for the site.

The borehole GW075409.1.2 at Thirlmere Lakes produced positive M_2 phase shifts (Table 2), with specific storage and hydraulic conductivity therefore being derived from the leaky model (Section 2.2.4). Both the quartz sandstone bores returned

405   *Biot-Willis* coefficients of 0.96 which requires a value for the grain compressibility (Section 2.4.3).

Estimates of hydro-geomechanical parameters (S_s of $3.2 \cdot 10^{-6}$ and $2.8 \cdot 10^{-6}$ (1/m); k^f of $4.8 \cdot 10^{-7}$ and $1.9 \cdot 10^{-5}$ (m/s)) for the two sandstone bores are considered realistic for a quartz sandstone in this area. The higher k^f for Thirlmere 2 is believed to be indicative of enhanced hydraulic conductivity due to fractures. For this sandstone formation, SCA (2005, 2006) has previously reported S_s values of $2.49 \cdot 10^{-6}$ to $2.41 \cdot 10^{-4}$ (1/m) and k^f of $1.15 \cdot 10^{-6}$ to $3.36 \cdot 10^{-6}$ (m/s) within this

410   formation, including fracture networks (Ross, 2014). Our estimate of the shear modulus of 2.6 GPa marginally exceeds the expected range of $1-2$ GPa (Bertuzzi, 2014; Zhang et al., 2016; Zhang and Lu, 2018). Conversely, the bulk modulus and Young's modulus both fall within the expected ranges of 2.6 to 5.3 and 3 to 8 GPa, respectively. The estimated Poisson's ratios of -0.64 and -0.03 are low compared to values between 0.2 and 0.3 typically measured in the laboratory (McMillan et al., 2019).

415   ## 3.4   Dodowa (Ghana)

Dodowa is located in the Shai Osudoku District in the southeastern part of the Greater Accra Region, Ghana. The local geology consists of the Togo Structural and Dahomeyan Structural units. The Togo being composed of a series of metamorphic and folded quartzites, phyllites and schists, and the Dahomeyan composed of altered belts of acid and basic gneisses. BH11 used within this paper is located in a Dahomeyan gneiss (Attoh et al., 1997). All units within the region appear highly weathered,

420   resulting in an 5 m unconsolidated regolith, confining the underlying fractured igneous and metamorphic units.

BH11 was installed and previously studied by Foppen et al. (2020), including atmospheric tide analysis. The time-series for the water levels of BH11 was collected at 20 min intervals between the 18/10/2016 and 07/06/2017 using Mini-Diver DI501 (Schlumberger pressure transducers), with atmospheric pressure being recorded with a Mini-Diver DI500 (Schlumberger barometric diver), located above ground (Foppen et al., 2020).

425   The gneiss bore returned a *Biot-Willis* coefficient of 0.84, and therefore required a value for the grain compressibility (Section 2.4.3).

The hydrogeomechanical estimates of hydraulic conductivity of $2.6 \cdot 10^{-6}$ (m/s) and specific storage of $7.2 \cdot 10^{-7}$ (1/m) are comparable with the values for the Togo Structural Unit from Foppen et al. (2020) derived from pumping and slug tests, which indicated ranges between 10^{-5} to 10^{-6} (m/s), and $2.3 \cdot 10^{-7}$ to $7.7 \cdot 10^{-8}$ (1/m), respectively. The estimated porosity of 0.08

430   for BH11 slightly exceeds the range of 0.005 to 0.05 in Foppen et al. (2020). Comparison of elastic modulus is problematic for schists, as values are dependent on the original protolith and may vary significantly, and because schistose rock masses
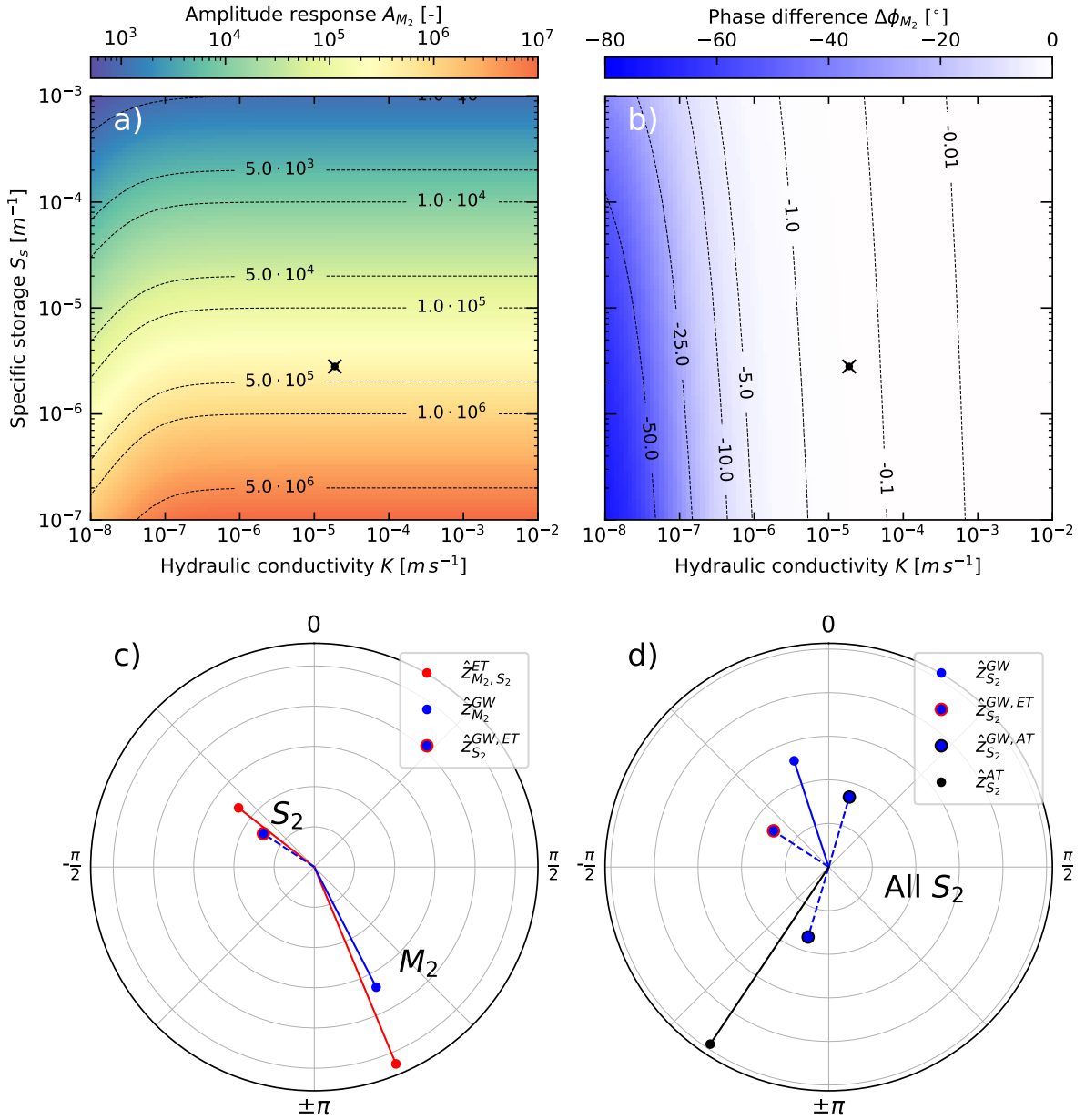
Figure 5. ~~Phase and~~ _Example_ amplitude ~~responses from the processing of bore Thirlmere 2 (black dot);~~ a) and _phase_ (b) ~~plot the theoretical amplitude ratio and phase shift relationships between the subsurface pore pressure and well water level~~ _responses calculated_ for _borehole Thirlmere 2 (black dots) using_ the confined Earth tide model (Section 2.2.3)~~, c) and d) are~~ _. The_ polar plots ~~showing~~ _show_ the amplitude and phases of the complex inference of the well response to Earth tides from the response at M_2 _(c)_, and the disentanglement of the well response at atmospheric tide S_2 ~~, respectively~~_(d)_.

are known for high values of anisotropy (Hoek and Diederichs, 2006). For example, Young's modulus for a schist, as in the screened interval of BH11, can vary significantly between 21 to 117 GPa depending on mineralogy and foliation orientation (Condon et al., 2020). Our estimated value of 34.2 GPa falls within this range. However, detailed mineralogy does not exist for this bore to allow a closer comparison with literature values.

3.5 Death Valley (California, USA)

The Death Valley site is located in the western part of the USA on the border of Nevada and California. Bore BLM-1 is located in Paleozoic carbonate rock and was left as an open well. The same time-series record was also used in Rau et al. (2020) and it is the same bore for which data was analysed in Cutillo and Bredehoeft (2011). Data was recorded at 15 min intervals using an In Situ Troll with a vented cable and an In Situ Barotroll. The time-series spans between the 25/06/2009 and 16/12/2009.

As the Death Valley dataset has previously been analysed by Rau et al. (2020) who justified the use of confined ET, this method was used for the -1 degree phase shift of the Death Valley dataset which is located in the limit between leaky and confined models.

The estimated hydraulic conductivity of $4.3 \cdot 10^{-6}$ (m/s), is in agreement with the Earth tide analysis derived value of $1.3 \cdot 10^{-6}$ (m/s) by Cutillo and Bredehoeft (2011). In contrast, the estimated specific storage value of $6.7 \cdot 10^{-7}$ $(1/m)$ is an order of magnitude smaller than the value of $7.3 \cdot 10^{-6}$ $(1/m)$ from Cutillo and Bredehoeft (2011). However, the specific storage and hydraulic conductivity values are both consistent with the values published by Rau et al. (2020) for the same data-set, using a method based on ET. The determined porosity (0.06) also aligns with the lower end of the range proposed by Cutillo and Bredehoeft (2011), and it is reasonable to assume the calculated Young's and shear modulus of 28.28 and 24.10 GPa are similarly plausible as they compare with literature values (Parent et al., 2015). We note that the derived Poisson's ratio of -0.23 differs significantly from the value of 0.25 which was merely assumed in Cutillo and Bredehoeft (2011).

4 Discussion

4.1 Influences on the ~~parameter estimation~~quantification of properties

While quantifying hydro-geomechanical properties it is beneficial to consider factors that influence the accuracy of parameter estimation. We note that absolute errors (i.e. offsets) in the measurement of atmospheric or groundwater pressure are irrelevant for the presented methodology. This is because all parameters are based on the amplitude and phase of tidal components embedded within the measurements, i.e., the relative change characteristic of the harmonics. Here, the resolution of the measurement device directly determines detection and quantification of the responses to tidal forces. Schweizer et al. (2021) demonstrated that extraction of harmonics using HALS is accurate if the resolution of the pressure transducer is larger than twice the amplitude of the tidal component under consideration. All instruments deployed in the field examples of this work comfortably fulfilled this criterion. Schweizer et al. (2021) further noted that HALS outperforms the discrete Fourier transform, but also that devising an objective error estimation for HALS is difficult, as it depends on the nature of the residuals (difference between

measurement and model), and this requires ~~separate~~ further investigation. We consider that the accuracy of HALS is at least as good as that resulting from fitting a conceptual model to measurements obtained during standard aquifer testing.

465 Previous works have illustrated that quantifying BE by disentangling the groundwater response to EAT based on theoretical Earth tides does not lead to additional uncertainty in parameter estimation since it evaluates the relative responses between ET and GW (Acworth et al., 2016). However, this observation is valid only in a subsurface where the hydraulic conductivity is $< K > \gtrsim 1 \cdot 10^{-5}$ m/s (Rau et al., 2020). The borehole water level response in lower $< K >$ environments is damped and shifted compared to the pore pressure response outside the bore. A correction requires knowledge of both $< K >$ and S_s which

470 can be quantified using calculated ET strains. While this has been done before (Hsieh et al., 1987; Xue et al., 2016; Allègre et al., 2016; Rau et al., 2020), there is no literature investigating its associated uncertainties.

4.2 Harmonic disentanglement allows estimation of the poroelastic parameter space

In this work, we make use of recent advances that allow quantitative disentanglement of the groundwater response to both Earth and atmospheric tidal forces. Since the two mechanisms acts differently on the subsurface, the disentangled responses

475 can be recombined to maximise the outcome. This allows the solving of the complete poroelastic space for unconsolidated systems entirely based on time-series of measured groundwater pressure heads, atmospheric pressure, and theoretical Earth tides. For consolidated systems, the complete poroelastic space can also be solved through a system of nonlinear equations by assuming a value for grain compressibility an approach previously used in Rau et al. (2018). While the results in Tables 3 and 4 provide reasonable values, except for the Poisson's ratio which is discussed separately below, they are difficult to validate

480 because independent measurements of poroelastic properties are rare.

It is well-established in the literature that a negative phase shift between strain and borehole water levels is representative of confined conditions and only horizontal flow between the formation and the bore (Bower, 1983; Hsieh et al., 1987; Kümpel, 1997; Schulze et al., 2000). Conversely, the meaning of positive phase shifts is not well established in the literature. Although Section 2.2.4 is based on the assumption that positive phase shifts relate to a component of vertical flow between the borehole

485 screen and the water table, i.e. semi-confined or leaky conditions (Roeloffs et al., 1989), other explanations for positive phase shifts exist within the literature. These include the influence of fracture transmissivity and length, the influence of ocean loading, heterogeneous material properties and topographic effects (Roeloffs, 1996; Burbey, 2010). Here, positive phases from either vertical flow or fracture flow describe a process in which pressure is able to be propagated rapidly, either to the water table or along a highly transmissive fracture (Bower, 1983). Other mechanisms for phase shifts have also been explored in

490 the broader literature, such as Hanson and Owen (1982), who related fracture orientation (strike and dip) to either positive or negative phase shifts.

Our results from various field sites show both positive and negative phase shifts. A comprehensive understanding of the causes and interpretation of phase shifts is still lacking within the scientific literature. Shi and Wang (2016) observed that negative phase shifts were indicative of predominantly horizontal groundwater flow in a completely undrained system, while

495 a positive phase shift was indicative of a vertical flow in a semi-confined or unconfined system. The method by Hsieh et al. (1987) outlined above as the confined model (negative phase shift), which was used by Shi and Wang (2016), is based on

the assumption of radial horizontal flow into a well. If a positive rather than negative phase shift is used as an input into the system of equations provided by Hsieh et al. (1987), the results will not be sensible. As such, a positive phase shift model is required. For this project the method provided by Wang (2000), and adapted by Xue et al. (2016) and Allègre et al. (2016), was implemented to account for vertical flow. Both Equation 13 and 14 were developed for harmonic loading (i.e. ocean or barometric loading) where strain is produced at the Earth's surface and propagated down (Wang and Davis, 1996). Earth tides do not act by surface loading but rather the mechanism is tidal dilatation, where gravitational forces act directly on all mass across the vertical profile. This points to possible issues with simplified conceptual models and the validity of their assumptions. Further research is required to ~~test the applicability of analytical solutions~~ independently validate results derived from passive methods that are based on simplified ~~assumptions applied to~~ conceptual understanding and their analytical solutions and to test the influence of different and more complex real-world conditions, such as geological heterogeneity at different scales.

4.3 Strain responses reveal subsurface heterogeneity and anisotropy

Combining ET and AT responses in the subsurface analysis is based on the principle that Earth and atmospheric tides induce strains with a different directionality. ET is fundamentally cubic, but is approximated as planar (tidal dilatation or strain) (Schulze et al., 2000; Fuentes-Arreazola et al., 2018). However, Rojstaczer and Agnew (1989) stated that the use of the horizontal areal strain from Earth tides is a sufficient approximation for subsurface depths of up to thousands of kilometres which should cover depths that are relevant to most groundwater systems. For ET, the well water levels must respond to strain in the vicinity of the well bore screen, although the sensitivity to strain that is more distant from the screen is unknown. The subsurface strain response to Earth tide induced stress depends on the elastic properties which are highly heterogeneous on a small scale. However, the pore pressure response as measured by a well intersects a larger volume and should therefore be representative of the theoretical values derived from Earth tide calculations.

Rojstaczer and Agnew (1989) predicted that the groundwater response to ET (areal strain) should be high for low porosity and low compressibility. Similarly, for such conditions, the barometric efficiency should approach one ($BE \rightarrow 1$, or equivalently $\gamma \rightarrow 0$). However, this is not reflected in our results for Death Valley and Dodowa where the groundwater response magnitude to ET is large but BE is significantly smaller than unity. This phenomenon can be explained by the fact that BE is estimated vertically across a typical geological profile as a surface load, uni-axially compressing the subsurface. Here, consolidation generally increases with depth and we hypothesise that the AT response vertically integrates the material properties above the well screen, i.e. the result is representative of the vertical heterogeneity in elastic properties encountered. The precise geometry of the representative volume from either ET or AT is currently unknown, but it is assumed to be equivalent. However, if this assumption is flawed and the representative volumes of ET or AT significantly differ, strain anisotropy may exist between these two forces and complicate their joint interpretation. Detailed field experimentation or coupled hydraulic-geomechanical modelling would be required to explore these processes.

4.4 Possible reasons for discrepancy in poroelastic properties

Our results in Tables 3 and 4 largely comply with previously established values (Wang, 2000), except for the observation of negative Poisson's ratios. It is important to note that previous studies typically assume a literature value for Poisson's ratio when calculating geomechanical properties (Cutillo and Bredehoeft, 2011). Our new approach based on tidal disentanglement removes the need for such an assumption. However, the negative Poisson ratios are a surprising result and require explanation. We investigated whether the influence from ocean tide loading could be responsible. However, considering the maximum possible influence from ocean tide loading for each site did not lead to positive Poisson's ratios.

It is theoretically possible for Poisson's ratio to range between $-1 \leq \nu \leq 0.5$ (Lakes, 1991; Lakes and Witt, 2002). Here, materials with a negative Poisson's ratio are described as auxetic, i.e. materials that become thicker parallel to the direction of the stress. The occurrence of auxetic behaviour in rocks was discussed by Gercek (2007), who summarised that as a Poisson's ratio becomes increasingly negative ($\nu \to -1$), the material becomes highly resistant to shear deformations but easy to deform volumetrically. Ji et al. (2018) succinctly describe this relationship for conditions where the shear modulus is much greater than the bulk modulus, defined as $K < 2G/3$, and geologically is likely associated with highly anisotropic rocks. This ratio between the bulk and shear modulus is consistent with all results presented in this paper. As such, the negative Poisson's ratios are indicative of the subsurface laterally contracting while being vertically compressed, following the theory of linear poroelasticity.

Negative Poisson's ratios for standard uniaxial core sample testing in thermally induced micro-cracked granites have previously been reported (Homand-Etienne and Houpert, 1989; Zhao et al., 2020). However, auxetic behaviour in rock is predominantly found in studies involving low strains and low confining pressures. For example, in the Berra Sandstone, Handin et al. (1963) observed that small compressive strains (i.e., less than 200 Bar $\approx 2000 \ mH_2O$ or 20 MPa) for confining pressure conditions cause the dilatation of pore spaces. Similarly, observations of pore volumes remained constant for moderate strains (20 to 50 MPa) and reduced in volume for large strains (> 50 MPa). Ji et al. (2018) have recently examined auxetic behaviour over a broad range of lithologies and pressures. They concluded that negative Poisson's ratios are possible in crystalline igneous and metamorphic rocks (non-fractured) for confining hydrostatic pressures less than 5 MPa, and less than 200–300 MPa for more quartz-rich sedimentary rocks such as silt stones and sand stones. Further, Ji et al. (2018) observed that the porosity of sedimentary rocks plays an important role in controlling auxetic effects, similar to the nano-scale fabric in artificial auxetic materials (e.g. metallic foams).

The results in this paper are obtained in-situ for fully saturated and leaky or confined conditions and caused by small magnitude strains. Such conditions differ considerably from those used in traditional laboratory techniques for determining elastic moduli (i.e., E, G, K, ν). Compared to the conditions experienced during a compressive laboratory test, or those described above by (Ji et al., 2018), the strains caused by EAT are very small. For example, the loading variations caused by the atmospheric tidal component S_2 is typically less than $9 \cdot 10^{-5}$ MPa (0.1 mH_2O), and the confining pressure caused by an artesian standing water level of 100 mH_2O equates to a confining pressure of only 0.98 MPa. Laboratory results are also well known for demonstrating bias in the sample strength, with the strength decreasing with the sample's increasing physical size.

It has been found that this occurs due to the incorporation of more heterogeneity in the sample at larger scales, such as minor lithological changes or discontinuities due to fracturing or jointing (Cundall et al., 2008; Masoumi et al., 2016).

Alternative in-situ methods, such as seismic based methods (Rau et al., 2018), derived positive Poisson's ratios when passing through the same heterogeneous material at the same confining pressures. However, elastic moduli have previously been shown to be frequency dependent when saturated and under confining pressure (Wang, 1993; Tutuncu et al., 1998). Here, we hypothesise that the low frequency of the EAT induced stresses (2 cpd $\approx 2.3 \cdot 10^{-5}$ Hz), compared to seismic propagated waves (1 to 100 $Hz \approx 86,400$ to $8,640,000$ cpd), causes a highly relaxed response which allows sufficient time for pressure redistribution (Tutuncu et al., 1998). In contrast, the seismic frequency produces a localised un-relaxed or un-drained response as the seismic waves pass through the subsurface, where this effect has been shown to change with the frequency (Pimienta et al., 2016). Both Tutuncu et al. (1998) and Pimienta et al. (2016) provide evidence of decreasing Poisson's ratios with decreasing frequency when below the typical undrained response domain (< 10 $Hz \approx 864,000$ cpd).

For small strains, as relevant for this study, Zaitsev et al. (2017) have shown that the occurrence of negative Poisson's ratios is not as exotic as previously thought. Considering the context of Cundall et al. (2008), Gercek (2007) and Ji et al. (2018), the negative Poisson's ratios derived by TSA in this paper seem plausible. We propose the following possible reasons which could lead to negative Poisson ratios hypotheses for conditions, such as the scale of the effective sample size, anisotropic strain responses from heterogeneities, low confining pressures, the low frequency and small strains caused by EATs, and boundary effects. Meeting the requirements of a negative Poisson's ratio at these small strains defined by (Lakes, 1991) as non-affine deformation (non-uniform between scales), non-central forces, and in a state of pre-existing strain (e.g., from overburden). The geomechanical derivations of this paper (Section 2.4) are based on linear poroelasticity. However, the auxetic responses observed by Ji et al. (2018) occurs both linearly and non-linearly within the negative Poisson's ratio space, depending on the confining pressure and the type of material (Zaitsev et al., 2017). Currently, no relationships between EAT and nonlinear poroelastic theory has been established within the literature. Future work in this space should therefore consider the integration of nonlinear geomechanics (Khan et al., 1991; Johnson and Rasolofosaon, 1996).

To the best knowledge of the authors no explicit or robust relationships exist in the literature between elastic moduli results obtained in the field to those estimated from the laboratory testing of core (Leriche, 2017). Similarly, no in-situ method currently exists that can derive elastic estimates representative of the large volume of material, such as surrounding a well bore screen, as has been proposed for Earth tides (Zhang et al., 2019). It is likely that heterogeneity within almost any geological media will produce an anisotropic strain response to either Earth or atmospheric tides over such a large volume. Anisotropy may result in apparently atypical properties, for example negative Poisson's ratios, and should be investigated for the validity of generic assumptions common to most hydro- or geomechanical investigations of a homogeneous, isotropic aquifer of infinite lateral extent.

4.5 Implications for passive quantification of subsurface hydro-geomechanical properties

There are several uncertainties associated with the findings of this paper, with implications for passive quantification of subsurface hydro-geomechanical properties. These uncertainties and limitations of the method are as follows:

- Although subjective estimates have been attempted (Zhang et al., 2019), the size and scale of the volume of influence from either ET or AT are unknown. It is also possible that there is a difference between the size of influence for ET and AT. Further research is required to elucidate the zone of influence the derived properties are representative for, such as by numeric modelling.

- Currently the poroelastic response to EAT is considered to be linear. However, rocks have previously been shown to respond in a nonlinear manner for undrained, tri-axially loaded laboratory settings, particularly at small strains (Johnson and Rasolofosaon, 1996; Zaitsev et al., 2017). As in-situ derivations of rock mass (or sediment) poroelastic values without assuming one or more of the primary values (E, G, K, ν) is relatively novel, the implication of assuming linearity for the analysis of in-situ properties remains unknown.

- The mechanism behind leaky responses is believed to be due to a partial drained response in the subsurface. However, the exact causes of such responses are still unknown. In order for the validity of a positive phase shift model to be proven, a more comprehensive understanding of such mechanisms must be further developed.

- Skin and well bore storage effects have been assumed to be negligible in this paper. However, these two effects will alter the phase responses to either Earth or atmospheric tides, as was shown in the recent work by Gao et al. (2020). It is important to note that any phase uncertainties mainly influence the hydraulic conductivity values. However, additional consideration of skin and well bore storage effects will increase the accuracy and confidence in results.

- We note that there is very little literature reporting values let alone ranges of grain compressibility for mineralogy other than quartz, as has been discussed by Rau et al. (2018). Since this is the only real unknown, further work is required to elucidate the effect of grain compressibility uncertainty on the accuracy of the parameter estimation.

Passively characterising the subsurface using the groundwater response to natural signals may improve our understanding of the subsurface. For example, the possibility of auxetic behaviour of subsurface materials in undrained conditions (i.e. hydraulically coupled) will have implications for assessing compaction from groundwater estimates, or the stability of slopes and cuttings. Here, the low strain elastic estimates from TSA may provide a lower bounding end-member for plausible ranges of properties. With further study, it may be possible to infer poroelastic properties at different confining pressures and frequencies or to provide a more accurate in-situ determination of geomechanical rock properties (e.g. specific storage, strength, etc.) prior to excavation and construction of civil and mining projects. However, further research is required to elucidate the scope of validity (space and time) and transferability of hydro-geomechanical properties derived from different methods.

5 Conclusions

The method developed in this paper provides a comprehensive approach to estimate in-situ hydro-geomechanical properties using Tidal Subsurface Analysis (TSA), i.e. from the monitored groundwater response to Earth and atmospheric tides (EAT). Our new method first objectively disentangles the groundwater response to Earth tides (ET) and atmospheric tides (AT) for

the dominant response frequencies (M_2 and S_2). Secondly, the approach uses the amplitude and phase responses to ET and AT to determine the complete hydro-geomechanical parameter space: Specific storage, hydraulic conductivity, porosity, shear, Young's and bulk modulus, undrained and drained Poisson's Ratio, Skempton's and Biot-Willis coefficients. Unlike previous research, our new approach does not require an a priori estimate of the Poisson's ratio. However, the application to consolidated systems requires an estimate for the grain compressibility for which literature based values can be considered if available.

Application of our new method to five groundwater and barometric pressure records from four different hydrogeological settings delivers physically realistic results that are consistent with previous estimates. However, we reveal that the in-situ estimates of Poisson's ratio are consistently negative indicating auxetic behaviour. A closer look at the literature reveals that this is not unrealistic and can be attributed to an interplay between simultaneous in-situ conditions that differ from those of established laboratory tests. These include a larger effective sample size with scaling effects, anisotropic strain responses due to heterogeneities (e.g., micro-cracking), significantly lower confining pressures, and the small strains at low frequencies caused by the EATs.

Our approach allows estimation of the complete hydro-geomechanical parameter space in a passive way, i.e. from monitoring records of groundwater pressure head, measured atmospheric pressure and calculated ET. The primary advantage is that all parameters are determined for the same in-situ conditions and that the estimated values therefore should be internally consistent. The new method ~~enables site-specific heterogeneity to be evaluated, as was shown by the two evaluated records from sandstone bores, providing~~ provides hydro-geomechanical properties of the ~~rock mass rather than small scale estimates on intact rock~~ larger rock mass. This is a clear advantage to methods that require taking samples to the laboratory where replicating field conditions such as in-situ confining pressure and representative scale can be problematic. When combined with laboratory estimates on intact rock, it enables evaluation of scale-specific heterogeneity. Further, our method enables more monitoring bores to be tested for hydro-geomechanical properties at a lower cost compared to conventional aquifer pump testing. There is thus the possibility of better characterizing the heterogeneity of aquifer properties. However, our method also raises the need for further research in key areas where significant uncertainties remain, for example the possibility for non-linearity of the poroelastic response to surface loading and Earth tide forces. Addressing the identified uncertainties could contribute towards improving subsurface monitoring and characterisation in both consolidated and unconsolidated systems.

Code and data availability. Data and code will be made available in a repository if this work is accepted for publication.

Author contributions. TCM and GCR conceived the idea for this paper. TCM and GCR analysed the data and made the figures. MSA and WAT contributed with datasets and suggested improvements.

Competing interests. The authors declare no competing interests.

Acknowledgements. Thanks are due to Francis Andorful, George Lutterodt, and Jan Willem Foppen from the T-GroUP project for drilling observation well BH11, installing a diver, and permitting the use of the Dodowa groundwater hydrograph data. We thank Paula Cutillo and Shannon Mazzei from the National Park Service (NPS) in California (USA) for providing the barometric and groundwater pressure dataset for BLM-1. We thank Hans-Georg Scherneck and Machiel Bos from Chalmers University of Technology for providing the ocean tide loading strains used in this manuscript. Some of the data used in this paper were collected with equipment provided by the Australian Federal Government financed *National Collaborative Research Infrastructure Strategy* (NCRIS). This project has received funding from the European Union's Horizon 2020 research and innovation programme under the Marie Skłodowska-Curie grant agreement No 835852. TCM was partly supported by an Australian Government Research Training Program (RTP) Scholarship. We acknowledge support by the KIT-Publication Fund of the Karlsruhe Institute of Technology.

660

665 References

Acworth, R. I., Timms, W. A., Kelly, B. F., Mcgeeney, D. E., Ralph, T. J., Larkin, Z. T., and Rau, G. C.: Late Cenozoic paleovalley fill sequence from the Southern Liverpool Plains, New South Wales—implications for groundwater resource evaluation, Australian Journal of Earth Sciences, 62, 657–680, https://doi.org/10.1080/08120099.2015.1086815, 2015.

Acworth, R. I., Halloran, L. J. S., Rau, G. C., Cuthbert, M. O., and Bernardi, T. L.: An objective frequency domain method for
670   quantifying confined aquifer compressible storage using Earth and atmospheric tides, Geophysical Research Letters, 43, 611–671, https://doi.org/10.1002/2016GL071328, http://dx.doi.org/10.1002/2016GL071328, 2016.

Acworth, R. I., Rau, G. C., Halloran, L. J. S., and Timms, W. A.: Vertical groundwater storage properties and changes in confinement determined using hydraulic head response to atmospheric tides, Water Resources Research, 53, 2983–2997, https://doi.org/10.1002/2016WR020311, http://dx.doi.org/10.1002/2016WR020311, 2017.

675 Agnew, D. C.: Earth Tides, Geodesy: Treatise on Geophysics, p. 163, 2010.

Allègre, V., Brodsky, E. E., Xue, L., Nale, S. M., Parker, B. L., and Cherry, J. A.: Using earth-tide induced water pressure changes to measure in situ permeability: A comparison with long-term pumping tests, Water Resources Research, 52, 3113–3126, https://doi.org/10.1002/2015WR017346, http://doi.wiley.com/10.1002/2015WR017346, 2016.

Attoh, K., Dallmeyer, R. D., and Affaton, P.: Chronology of nappe assembly in the Pan-African Dahomeyide orogen, West Africa: evidence
680   from 40Ar39Ar mineral ages, Precambrian Research, 82, 153–171, https://doi.org/https://doi.org/10.1016/S0301-9268(96)00031-9, http://www.sciencedirect.com/science/article/pii/S0301926896000319, 1997.

Barr, A. G., van der Kamp, G., Schmidt, R., and Black, T. A.: Monitoring the moisture balance of a boreal aspen forest using a deep groundwater piezometer, Agricultural and Forest Meteorology, 102, 13–24, 2000.

Beavan, J., Evans, K., Mousa, S., and Simpson, D.: Estimating aquifer parameters from analysis of forced fluctuations in well level: An
685   example from the Nubian Formation near Aswan, Egypt: 2. Poroelastic properties, Journal of Geophysical Research: Solid Earth, 96, 12 139–12 160, https://doi.org/10.1029/91JB00956, https://doi.org/10.1029/91JB00956, 1991.

Bertuzzi, R.: Sydney sandstone and shale parameters for tunnel design, Australian Geomechanics Journal, 49, 1–39, 2014.

Bouzalakos, S., Crane, R. A., McGeeney, D., and Timms, W. A.: Stress-dependent hydraulic properties of clayey-silt aquitards in eastern Australia, Acta Geotechnica, 11, 969–986, 2016.

690 Bower, D. R.: Bedrock fracture parameters from the interpretation of well tides, Journal of Geophysical Research: Solid Earth, 88, 5025–5035, https://doi.org/10.1029/JB088iB06p05025, https://doi.org/10.1029/JB088iB06p05025, 1983.

Bowles, L. E.: Foundation analysis and design, McGraw-hill, 1996.

Bredehoeft, J. D.: Response of well-aquifer systems to Earth tides, Journal of Geophysical Research, 72, 3075–3087, https://doi.org/10.1029/JZ072i012p03075, http://doi.wiley.com/10.1029/JZ072i012p03075, 1967.

695 Burbey, T. J.: Fracture characterization using Earth tide analysis, Journal of Hydrology, 380, 237 – 246, https://doi.org/https://doi.org/10.1016/j.jhydrol.2009.10.037, http://www.sciencedirect.com/science/article/pii/S0022169409007069, 2010.

Burbey, T. J., Hisz, D., Murdoch, L. C., and Zhang, M.: Quantifying fractured crystalline-rock properties using well tests, earth tides and barometric effects, Journal of Hydrology, 414, 317–328, https://doi.org/10.1016/j.jhydrol.2011.11.013, http://linkinghub.elsevier.com/retrieve/
700   pii/S002216941100789X, 2012.

Clark, W. E.: Computing the barometric efficiency of a well, Journal of the Hydraulics Division, 93, 93–98, http://cedb.asce.org/CEDBsearch/record.jsp?dockey=0014622, 1967.

Condon, K. J., Sone, H., Wang, H. F., Ajo-Franklin, J., Baumgartner, T., Beckers, K., Blankenship, D., Bonneville, A., Boyd, L., Brown, S., Burghardt, J. A., Chai, C., Chen, Y., Chi, B., Condon, K., Cook, P. J., Crandall, D., Dobson, P. F., Doe, T., Doughty, C. A., Elsworth, D., Feldman, J., Feng, Z., Foris, A., Frash, L. P., Frone, Z., Fu, P., Gao, K., Ghassemi, A., Guglielmi, Y., Haimson, B., Hawkins, A., Heise, J., Hopp, C., Horn, M., Horne, R. N., Horner, J., Hu, M., Huang, H., Huang, L., Im, K. J., Ingraham, M., Jafarov, E., Jayne, R. S., Johnson, S. E., Johnson, T. C., Johnston, B., Kim, K., King, D. K., Kneafsey, T., Knox, H., Knox, J., Kumar, D., Lee, M., Li, K., Li, Z., Maceira, M., Mackey, P., Makedonska, N., Mattson, E., McClure, M. W., McLennan, J., Medler, C., Mellors, R. J., Metcalfe, E., Moore, J., Morency, C. E., Morris, J. P., Myers, T., Nakagawa, S., Neupane, G., Newman, G., Nieto, A., Oldenburg, C. M., Paronish, T., Pawar, R., Petrov, P., Pietzyk, B., Podgorney, R., Polsky, Y., Pope, J., Porse, S., Primo, J. C., Reimers, C., Roberts, B. Q., Robertson, M., Roggenthen, W., Rutqvist, J., Rynders, D., Schoenball, M., Schwering, P., Sesetty, V., Sherman, C. S., Singh, A., Smith, M. M., Sone, H., Sonnenthal, E. L., Soom, F. A., Sprinkle, P., Strickland, C. E., Su, J., Templeton, D., Thomle, J. N., Tribaldos, V. R., Ulrich, C., Uzunlar, N., Vachaparampil, A., Valladao, C. A., Vandermeer, W., Vandine, G., Vardiman, D., Vermeul, V. R., Wagoner, J. L., Wang, H. F., Weers, J., Welch, N., White, J., White, M. D., Winterfeld, P., Wood, T., Workman, S., Wu, H., Wu, Y. S., Yildirim, E. C., Zhang, Y., Zhang, Y. Q., Zhou, Q., Zoback, M. D., and CollabTeam, E. G. S.: Low Static Shear Modulus Along Foliation and Its Influence on the Elastic and Strength Anisotropy of Poorman Schist Rocks, Homestake Mine, South Dakota, Rock Mechanics and Rock Engineering, 53, 5257–5281, https://doi.org/10.1007/s00603-020-02182-4, https://doi.org/10.1007/s00603-020-02182-4, 2020.

Cundall, P. A., Pierce, M. E., and Mas Ivars, D.: Quantifying the Size Effect of Rock Mass Strength, https://papers.acg.uwa.edu.au/p/808_31_Cundall/, 2008.

Cutillo, P. A. and Bredehoeft, J. D.: Estimating Aquifer Properties from the Water Level Response to Earth Tides, Ground Water, 49, 600–610, https://doi.org/10.1111/j.1745-6584.2010.00778.x, http://doi.wiley.com/10.1111/j.1745-6584.2010.00778.x, 2011.

Foppen, J. W., Lutterodt, G., Rau, G. C., and Minkah, O.: Groundwater flow system analysis in the regolith of Dodowa on the Accra Plains, Ghana, Journal of Hydrology: Regional Studies, 28, 100 663, https://doi.org/https://doi.org/10.1016/j.ejrh.2020.100663, http://www.sciencedirect.com/science/article/pii/S2214581819300552, 2020.

Fuentes-Arreazola, M., Ramírez-Hernández, J., and Vázquez-González, R.: Hydrogeological Properties Estimation from Groundwater Level Natural Fluctuations Analysis as a Low-Cost Tool for the Mexicali Valley Aquifer, Water, 10, 586, https://doi.org/10.3390/w10050586, http://www.mdpi.com/2073-4441/10/5/586, 2018.

Gao, X., Sato, K., and Horne, R. N.: General Solution for Tidal Behavior in Confined and Semiconfined Aquifers Considering Skin and Wellbore Storage Effects, Water Resources Research, 56, e2020WR027 195, https://doi.org/10.1029/2020WR027195, https://doi.org/10.1029/2020WR027195, 2020.

Gercek, H.: Poisson's ratio values for rocks, International Journal of Rock Mechanics and Mining Sciences, 44, 1–13, https://doi.org/https://doi.org/10.1016/j.ijrmms.2006.04.011, http://www.sciencedirect.com/science/article/pii/S136516090600075X, 2007.

Gonthier, G.: A Graphical Method for Estimation of Barometric Efficiency from Continuous Data - Concepts and Application to a Site in the Piedmont, Air Force Plant 6, Marietta, Georgia, Tech. rep., US Geological Survey, https://doi.org/10.3133/sir20075111, https://pubs.er.usgs.gov/publication/sir20075111, 2003.

Green, D. H. and Wang, H. F.: Specific storage as a poroelastic coefficient, Water Resources Research, 26, 1631–1637, https://doi.org/10.1029/WR026i007p01631, https://doi.org/10.1029/WR026i007p01631, 1990.

Handin, J., Hager Jr, R. V., Friedman, M., and Feather, J. N.: Experimental deformation of sedimentary rocks under confining pressure: pore pressure tests, Aapg Bulletin, 47, 717–755, 1963.

Hanson, J. M. and Owen, L. B.: Fracture orientation analysis by the solid earth tidal strain method, in: Proceedings - SPE Annual Technical Conference and Exhibition, vol. 1982-Septe, p. 18, Society of Petroleum Engineers, New Orleans, Louisiana, https://doi.org/10.2118/11070-MS, http://www.onepetro.org/doi/10.2118/11070-MShttps://doi.org/10.2118/11070-MS, 1982.

Hoek, E. and Diederichs, M. S.: Empirical estimation of rock mass modulus, International Journal of Rock Mechanics and Mining Sciences, 43, 203–215, https://doi.org/https://doi.org/10.1016/j.ijrmms.2005.06.005, http://www.sciencedirect.com/science/article/pii/S1365160905000948, 2006.

Homand-Etienne, F. and Houpert, R.: Thermally induced microcracking in granites: characterization and analysis, International Journal of Rock Mechanics and Mining Sciences & Geomechanics Abstracts, 26, 125–134, https://doi.org/https://doi.org/10.1016/0148-9062(89)90001-6, http://www.sciencedirect.com/science/article/pii/0148906289900016, 1989.

Hsieh, P. A., Bredehoeft, J. D., and Farr, J. M.: Determination of aquifer transmissivity from Earth tide analysis, Water Resources Research, 23, 1824–1832, https://doi.org/10.1029/WR023i010p01824, http://doi.wiley.com/10.1029/WR023i010p01824, 1987.

Hsieh, P. A., Bredehoeft, J. D., and Rojstaczer, S. A.: Response of well aquifer systems to Earth tides: Problem revisited, Water Resources Research, 24, 468–472, https://doi.org/10.1029/WR024i003p00468, http://dx.doi.org/10.1029/WR024i003p00468http://doi.wiley.com/10.1029/WR024i003p00468, 1988.

Impax: Impax Drilling correspondance and drill reports: Thirlmere 1 and 2, Tech. rep., 2019.

Jacob, C. E.: On the flow of water in an elastic artesian aquifer, Eos, Transactions American Geophysical Union, 21, 574–586, 1940.

Jentzsch, G.: Earth tides and ocean tidal loading, pp. 145–171, Springer Berlin Heidelberg, Berlin, Heidelberg, https://doi.org/10.1007/BFb0011461, https://doi.org/10.1007/BFb0011461, 1997.

Ji, S., Li, L., Motra, H. B., Wuttke, F., Sun, S., Michibayashi, K., and Salisbury, M. H.: Poisson's Ratio and Auxetic Properties of Natural Rocks, Journal of Geophysical Research: Solid Earth, 123, 1161–1185, https://doi.org/10.1002/2017JB014606, https://doi.org/10.1002/2017JB014606, 2018.

Johnson, P. A. and Rasolofosaon, P. N. J.: Nonlinear elasticity and stress-induced anisotropy in rock, Journal of Geophysical Research: Solid Earth, 101, 3113–3124, https://doi.org/10.1029/95JB02880, https://doi.org/10.1029/95JB02880, 1996.

Khan, A. S., Xiang, Y., and Huang, S.: Behavior of Berea sandstone under confining pressure part I: Yield and failure surfaces, and nonlinear elastic response, International Journal of Plasticity, 7, 607–624, https://doi.org/https://doi.org/10.1016/0749-6419(91)90046-2, http://www.sciencedirect.com/science/article/pii/0749641991900462, 1991.

Kümpel, H.-J.: Tides in water saturated rock BT - Tidal Phenomena, pp. 277–291, Springer Berlin Heidelberg, Berlin, Heidelberg, https://doi.org/10.1007/BFb0011467, https://doi.org/10.1007/BFb0011467, 1997.

Lakes, R.: Deformation mechanisms in negative Poisson's ratio materials: structural aspects, Journal of Materials Science, 26, 2287–2292, https://doi.org/10.1007/BF01130170, https://doi.org/10.1007/BF01130170, 1991.

Lakes, R. S. and Witt, R.: Making and characterizing negative Poisson's ratio materials, International Journal of Mechanical Engineering Education, 30, 50–58, 2002.

Leriche, A.: Stress estimation from borehole scans for prediction of excavation overbreak in brittle rock., Ph.D. thesis, Kingston, Ontario, Canada: Queen's University, 2017.

775 Masoumi, H., Douglas, K. J., and Russell, A. R.: A Bounding Surface Plasticity Model for Intact Rock Exhibiting Size-Dependent Behaviour, Rock Mechanics and Rock Engineering, 49, 47–62, https://doi.org/10.1007/s00603-015-0744-8, http://link.springer.com/10.1007/s00603-015-0744-8, 2016.

Matviichuk, B., King, M. A., Watson, C. S., and Bos, M. S.: Limitations in One-Dimensional (an)Elastic Earth Models for Explaining GPS-Observed M sub2/sub Ocean Tide Loading Displacements in New Zealand, Journal of Geophysical Research: Solid Earth, 126,
780 https://doi.org/10.1029/2021jb021992, 2021.

McMillan, T. C., Rau, G. C., Timms, W. A., and Andersen, M. S.: Utilizing the Impact of Earth and Atmospheric Tides on Groundwater Systems: A Review Reveals the Future Potential, Reviews of Geophysics, 57, 281–315, https://doi.org/10.1029/2018RG000630, https://onlinelibrary.wiley.com/doi/abs/10.1029/2018RG000630, 2019.

Merritt, M. L.: Estimating hydraulic properties of the Floridan Aquifer System by analysis of earth-tide, ocean-tide, and barometric effects,
785 Collier and Hendry Counties, Florida, Tech. rep., https://doi.org/10.3133/wri034267, https://pubs.er.usgs.gov/publication/wri034267, 2004.

Miall, A. D. and Jones, B. G.: Fluvial architecture of the Hawkesbury sandstone (Triassic), near Sydney, Australia, Journal of Sedimentary Research, 4, 531–545, 2003.

Narasimhan, T. N., Kanehiro, B. Y., and Witherspoon, P. A.: Interpretation of Earth tide response of three deep, confined aquifers,
790 Journal of Geophysical Research: Solid Earth, 89, 1913–1924, https://doi.org/10.1029/JB089iB03p01913, http://doi.wiley.com/10.1029/JB089iB03p01913, 1984.

Parent, T., Domede, N., Sellier, A., and Mouatt, L.: Mechanical characterization of limestone from sound velocity measurement, 2015.

Penna, N. T., Bos, M. S., Baker, T. F., and Scherneck, H.-G.: Assessing the accuracy of predicted ocean tide loading displacement values, Journal of Geodesy, 82, 893–907, https://doi.org/10.1007/s00190-008-0220-2, 2008.

795 Pimienta, L., Fortin, J., and Guéguen, Y.: Effect of fluids and frequencies on Poisson's ratio of sandstone samples, Geophysics, 81, D183–D195, https://doi.org/10.1190/geo2015-0310.1, https://doi.org/10.1190/geo2015-0310.1, 2016.

Rasmussen, T. C. and Crawford, L. A.: Identifying and Removing Barometric Pressure Effects in Confined and Unconfined Aquifers, Ground Water, 35, 502–511, https://doi.org/10.1111/j.1745-6584.1997.tb00111.x, http://doi.wiley.com/10.1111/j.1745-6584.1997.tb00111.x, 1997.

800 Rau, G. C.: PyGTide: A Python module and wrapper for ETERNA PREDICT to compute synthetic model tides on Earth, https://doi.org/10.5281/zenodo.1346260, https://doi.org/10.5281/zenodo.1346260, 2018.

Rau, G. C., Acworth, R. I., Halloran, L. J. S., Timms, W. A., and Cuthbert, M. O.: Quantifying Compressible Groundwater Storage by Combining Cross-Hole Seismic Surveys and Head Response to Atmospheric Tides, Journal of Geophysical Research: Earth Surface, 123, 1910–1930, https://doi.org/10.1029/2018JF004660, https://doi.org/10.1029/2018JF004660http://doi.wiley.com/10.1029/2018JF004660,
805 2018.

Rau, G. C., Post, V. E. A., Shanafield, M., Krekeler, T., Banks, E. W., and Blum, P.: Error in hydraulic head and gradient time-series measurements: a quantitative appraisal, Hydrology and Earth System Sciences, 23, 3603–3629, https://doi.org/10.5194/hess-23-3603-2019, https://www.hydrol-earth-syst-sci-discuss.net/hess-2019-182/https://www.hydrol-earth-syst-sci.net/23/3603/2019/, 2019.

Rau, G. C., Cuthbert, M. O., Acworth, R. I., and Blum, P.: Technical note: Disentangling the groundwater response to Earth and atmospheric
810 tides to improve subsurface characterisation, Hydrology and Earth System Sciences, 24, 6033–6046, https://doi.org/10.5194/hess-24-6033-2020, 2020.

Richardson, N. D., Williams, K. L., Briggs, K. B., and Thorsos, E. I.: Dynamic measurement of sediment grain compressibility at atmospheric pressure: acoustic applications, IEEE Journal of Oceanic Engineering, 27, 593–601, https://doi.org/10.1109/JOE.2002.1040941, 2002.

Ritzi, R. W., Sorooshian, S., and Hsieh, P. A.: The estimation of fluid flow properties from the response of water levels in wells to the combined atmospheric and Earth tide forces, Water Resources Research, 27, 883–893, https://doi.org/10.1029/91WR00070, http://doi.wiley.com/10.1029/91WR00070, 1991.

Roeloffs, E.: Poroelastic Techniques in the Study of Earthquake-Related Hydrologic Phenomena, in: Advances in Geophysics, vol. 38, pp. 135–195, https://doi.org/10.1016/S0065-2687(08)60270-8, https://linkinghub.elsevier.com/retrieve/pii/S0065268708602708, 1996.

Roeloffs, E. A., Burford, S. S., Riley, F. S., and Records, A. W.: Hydrologic effects on water level changes associated with episodic fault creep near Parkfield, California, Journal of Geophysical Research, 94, 12 387, https://doi.org/10.1029/jb094ib09p12387, http://doi.wiley.com/10.1029/JB094iB09p12387, 1989.

Rojstaczer, S.: Determination of fluid flow properties from the response of water levels in wells to atmospheric loading, Water Resources Research, 24, 1927–1938, https://doi.org/10.1029/WR024i011p01927, 1988.

Rojstaczer, S. and Agnew, D. C.: The influence of formation material properties on the response of water levels in wells to Earth tides and atmospheric loading, Journal of Geophysical Research, 94, 12 403, https://doi.org/10.1029/JB094iB09p12403, http://doi.wiley.com/10.1029/JB094iB09p12403, 1989.

Rojstaczer, S. and Riley, F. S.: Response of the water level in a well to Earth tides and atmospheric loading under unconfined conditions, Water Resources Research, 26, 1803–1817, https://doi.org/10.1029/WR026i008p01803, 1990.

Ross, J. B.: Groundwater resource potential of the Triassic Sandstones of the Southern Sydney Basin: an improved understanding, Australian Journal of Earth Sciences, 61, 463–474, https://doi.org/10.1080/08120099.2014.910548, http://dx.doi.org/10.1080/08120099.2014.910548, 2014.

Russell, G.: Thirlmere Lakes drilling report, Tech. rep., NSW Office of Water, Sydney, 2012.

SCA: Metropolitan Water Plan. Priority Groundwater Investigations for Emergency Drought Relief. Area 2: Upper Nepean Catchment., Tech. rep., 2005.

SCA: Upper Nepean Groundwater Pilot Studies - Pumping Test Interpretation and Data Logger Installation, Tech. rep., 2006.

Schulze, K. C., Kümpel, H.-J., and Huenges, E.: In-Situ Petrohydraulic Parameters from Tidal and Barometric Analysis of Fluid Level Variations in Deep Wells: Some Results From KTB BT - Hydrogeology of Crystalline Rocks, pp. 79–104, Springer Netherlands, Dordrecht, https://doi.org/10.1007/978-94-017-1816-5_4, https://doi.org/10.1007/978-94-017-1816-5_4, 2000.

Schweizer, D., Ried, V., Rau, G. C., Tuck, J. E., and Stoica, P.: Comparing Methods and Defining Practical Requirements for Extracting Harmonic Tidal Components from Groundwater Level Measurements, Mathematical Geosciences, https://doi.org/10.1007/s11004-020-09915-9, 2021.

Shi, Z. and Wang, G.: Aquifers switched from confined to semiconfined by earthquakes, Geophysical Research Letters, 43, 111–166, https://doi.org/10.1002/2016GL070937, https://doi.org/10.1002/2016GL070937, 2016.

Timms, W. A. and Acworth, R. I.: Propagation of pressure change through thick clay sequences: an example from Liverpool Plains, NSW, Australia, Hydrogeology Journal, 13, 858–870, https://doi.org/10.1007/s10040-005-0436-7, http://link.springer.com/10.1007/s10040-005-0436-7, 2005.

Timms, W. A., Acworth, R. I., Crane, R. A., Arns, C. H., Arns, J., McGeeney, D. E., Rau, G. C., and Cuthbert, M. O.: The influence of syndepositional macropores on the hydraulic integrity of thick alluvial clay aquitards, Water Resources Research, 54, 3122–3138, 2018.

Turnadge, C., Crosbie, R. S., Barron, O., and Rau, G. C.: Comparing Methods of Barometric Efficiency Characterization for Specific Storage Estimation, Groundwater, 57, 844–859, https://doi.org/10.1111/gwat.12923, https://onlinelibrary.wiley.com/doi/abs/10.1111/gwat.12923, 2019.

Tutuncu, A. N., Podio, A. L., Gregory, A. R., and Sharma, M. M.: Nonlinear viscoelastic behavior of sedimentary rocks, Part I: Effect of frequency and strain amplitude, Geophysics, 63, 184–194, https://doi.org/10.1190/1.1444311, https://doi.org/10.1190/1.1444311, 1998.

Van Camp, M. and Vauterin, P.: Tsoft: graphical and interactive software for the analysis of time series and Earth tides, Computers & Geosciences, 31, 631–640, https://doi.org/10.1016/j.cageo.2004.11.015, http://linkinghub.elsevier.com/retrieve/pii/S0098300404002456, 2005.

van der Kamp, G. and Gale, J. E.: Theory of earth tide and barometric effects in porous formations with compressible grains, Water Resources Research, 19, 538–544, https://doi.org/10.1029/WR019i002p00538, http://dx.doi.org/10.1029/WR019i002p00538, 1983.

Villeneuve, M. C., Heap, M. J., Kushnir, A. R. L., Qin, T., Baud, P., Zhou, G., and Xu, T.: Estimating in situ rock mass strength and elastic modulus of granite from the Soultz-sous-Forêts geothermal reservoir (France), Geothermal Energy, 6, 11, https://doi.org/10.1186/s40517-018-0096-1, https://doi.org/10.1186/s40517-018-0096-1, 2018.

Wahr, J. M.: Body tides on an elliptical, rotating, elastic and oceanless earth, Geophysical Journal of the Royal Astronomical Society, 64, 677–703, https://doi.org/10.1111/j.1365-246X.1981.tb02690.x, https://academic.oup.com/gji/article-lookup/doi/10.1111/j.1365-246X.1981.tb02690.x, 1981.

Wang, H. F.: Quasi-static poroelastic parameters in rock and their geophysical applications, pure and applied geophysics, 141, 269–286, https://doi.org/10.1007/BF00998332, https://doi.org/10.1007/BF00998332, 1993.

Wang, H. F.: Theory of Linear Poroelasticity with Applications to Geomechanics and Hydrogeology, Princeton University Press, https://press.princeton.edu/titles/7006.html, 2000.

Wang, K. and Davis, E. E.: Theory for the propagation of tidally induced pore pressure variations in layered subseafloor formations, Journal of Geophysical Research: Solid Earth, 101, 11 483–11 495, 1996.

Wenzel, H.-G.: Accuracy assessment for tidal potential catalogues, Bulletin d'Informations des Marées Terrestres, 124, 9394–9416, 1996.

Xue, L., Brodsky, E. E., Erskine, J., Fulton, P. M., and Carter, R.: A permeability and compliance contrast measured hydrogeologically on the San Andreas Fault, Geochemistry, Geophysics, Geosystems, 17, 858–871, https://doi.org/10.1002/2015GC006167, https://doi.org/10.1002/2015GC006167, 2016.

Zaitsev, V. Y., Radostin, A. V., Pasternak, E., and Dyskin, A.: Extracting real-crack properties from non-linear elastic behaviour of rocks: abundance of cracks with dominating normal compliance and rocks with negative Poisson ratios, Nonlinear Processes in Geophysics, 24, 543–551, https://doi.org/10.5194/npg-24-543-2017, https://npg.copernicus.org/articles/24/543/2017/, 2017.

Zhang, C. and Lu, N.: What Is the Range of Soil Water Density? Critical Reviews With a Unified Model, Reviews of Geophysics, 56, 532–562, https://doi.org/10.1029/2018RG000597, http://doi.wiley.com/10.1029/2018RG000597, 2018.

Zhang, C., Mitra, R., Oh, J., and Hebblewhite, B.: Analysis of Mining-induced Valley Closure Movements, Rock Mechanics and Rock Engineering, 49, 1923–1941, https://doi.org/10.1007/s00603-015-0880-1, 2016.

Zhang, S., Shi, Z., and Wang, G.: Comparison of aquifer parameters inferred from water level changes induced by slug test, earth tide and earthquake – A case study in the three Gorges area, Journal of Hydrology, 579, 124 169, https://doi.org/https://doi.org/10.1016/j.jhydrol.2019.124169, http://www.sciencedirect.com/science/article/pii/S0022169419309047, 2019.

Zhao, Z., Xu, H., Wang, J., Zhao, X., Cai, M., and Yang, Q.: Auxetic behavior of Beishan granite after thermal treatment: A microcracking perspective, Engineering Fracture Mechanics, 231, 107 017, https://doi.org/https://doi.org/10.1016/j.engfracmech.2020.107017, http://www.sciencedirect.com/science/article/pii/S0013794420301636, 2020.